

Noise correlation tomography of Southwest Western Canada Sedimentary Basin

Yu Jeffrey Gu and Luyi Shen

Department of Physics, University of Alberta, Edmonton, AB, Canada T6G2E1. E-mail: ygu@ualberta.ca

Accepted 2015 February 26. Received 2015 February 7; in original form 2014 July 2

SUMMARY

We analyse continuous recordings from 23 broadband seismic stations near Alberta, the southwestern sector of the Western Canada Sedimentary Basin. Noise correlation tomography based on vertical-component seismograms reveals below-average shear velocities at shallow and middle crustal depths in central Alberta, spanning across Proterozoic accreted terranes and Archean microcontinents. This observation likely results from extensive plate convergence and crustal melting during the Proterozoic eon. The overall correlation between the crustal velocities and presumed basement domains is lower than expected, however. In the lower crust, the main pattern of shear velocities is relatively concordant with the reported domain boundaries and key Precambrian structures appear to be intact. The shear velocities beneath the Loverna Block, the largest constituent of the Hearne craton, are 10 per cent higher than the regional average. This prominent northeast striking seismic anomaly is moderately correlated with the regional heat flow and potentially represents the remnant core of the Archean Hearne province. The associated high velocities extend into the western part of the Medicine Hat Block, a possible Archean microcontinent with a debatable origin, and contribute to a strong east–west structural gradient in the lower crust. The presence and the continuity of this anomalous structure imply extensive communications among the various basement domains in southern Alberta during the assembly of the North American continent.

Key words: Interferometry; Composition of the continental crust; Surface waves and free oscillations; Seismic tomography; Intra-plate processes; Cratons.

1 INTRODUCTION

The basement structure under the Western Canada Sedimentary Basin (WCSB) contains vital records of the Precambrian tectonic development of western Laurentia (Hoffman 1988, 1990; Ross *et al.* 1991; Villeneuve *et al.* 1993; Ross *et al.* 2000). Largely buried under a veneer of Phanerozoic sediments, the surface exposure of WCSB is mainly confined to the northeastern segments where geochemical signatures from the Archean Slave province have been identified (Frost & Burwash 1986; Hoffman 1988; Thériault & Ross 1991; Burwash *et al.* 2000; De *et al.* 2000; Canil *et al.* 2003; Cook *et al.* 2009). In comparison, the basement structure in southwestern WCSB, the main focus of this study, is much less accessible and may have undergone episodes of Archean and Palaeoproterozoic collisions among the Hearne, Rae, Superior and Wyoming provinces (Beaumont *et al.* 1994; Ross & Eaton 2002; Aulbach *et al.* 2004; Mahan & Williams 2005). The extensive tectonic history of Southwest WCSB culminated a diverse geological framework consisting of Archean cratons, Proterozoic orogens and accretionary margins known as ‘terranes’. Consequently, information pertaining to the basement structure beneath the various tectonic domains (Hoffman

1988; Ross *et al.* 1991) can provide critical insights into the assembly and evolution of the western boundary of the Canadian shield.

The intricate tectonic domains beneath Southwest WCSB have been investigated by regional gravity, magnetic and seismic surveys (Ross *et al.* 1991, 2000; Thériault & Ross 1991). Among the various approaches, the use of reflection seismic methods is particularly instrumental at mapping rock elastic properties, faults and reflective structures in the crust. In the early 1990s, a series of active-source seismic surveys was conducted as part of the LITHOPROBE project (Ross 2000). The Alberta Transect from this trans-Canada experiment contains three major reflection profiles totalling 1400 km in length (Eaton *et al.* 1999b; Lemieux *et al.* 2000; Ross *et al.* 2000). Additionally, reflection and refraction analyses based on the Alberta Basement Transect (ABT), Deep Probe, and Southern Alberta Refraction Experiment (SAREX; Clowes *et al.* 2002; Gorman *et al.* 2002) enabled the verification and refinement of the existing theories (Hoffman 1988) pertaining to the basement formation and evolution of Southwest WCSB (Zelt & Ellis 1989; Ross *et al.* 1995; Zelt & White 1995; Eaton & Cassidy 1996; Ross & Eaton 1997; Eaton *et al.* 1999b, 2000; Lemieux *et al.* 2000; Ross *et al.* 2000; Bouzidi *et al.* 2002; Ross & Eaton 2002). These efforts are

complemented by broadband seismic recordings from Canadian National Seismic Network (CNSN) stations (Cassidy 1995; Eaton & Cassidy 1996) and temporary deployments such as Canadian Northwest Experiment (CANOE; Mercier *et al.* 2008; Courtier *et al.* 2010; Dalton *et al.* 2011), BATHOLITHS (Mercier *et al.* 2009) and Florida-to-Edmonton Array (FLED; French *et al.* 2009), which offered improved data constraints at mantle depths. Analyses of the teleseismic data (e.g. Shragge *et al.* 2002; Mercier *et al.* 2008, 2009) raised critical questions on the state, history and integrity of the lithosphere (Shragge *et al.* 2002) beneath Southwest WCSB.

Despite the aforementioned progress, limited surface-exposed geology remains a formidable challenge in the accurate assessment of regional basement history of Southwest WCSB. Only local-scale, 2-D receiver geometries had been attempted prior to 2005 (Kanasewich *et al.* 1995), while the majority of the temporary experiments only lasted 1 year or less. These apparent drawbacks left much of the WCSB undersampled. Consequently, interpretations of the domain boundaries and tectonic history of this region relied heavily on electromagnetic (EM) and potential field observations (e.g. Ross *et al.* 1991, 2000; Boerner *et al.* 1999; Hope & Eaton 2002), which suffered from limited depth sensitivities as well as debatable relationships with seismic velocities.

The seismic data coverage was substantially improved by the establishment of the Canadian Rockies and Alberta Network (CRANE; Gu *et al.* 2011). This array of semi-permanent broadband stations is designed to complement the existing CNSN stations and provide near-uniform receiver coverage in central and southern Alberta, the main constituents of Southwest WCSB and the focus of this study. The seismic recordings from CRANE facilitated a number of new research initiatives in the investigations of regional seismic structures (Gu *et al.* 2011) and sources (e.g. Gu & Shen 2012; Schultz *et al.* 2014). Based largely on the array data, this study presents new results from an analysis of ambient seismic noise between stations. By exploiting frequency-dependent group velocities, our findings offer direct constraints on the existence and integrity of crustal domain structures and boundaries.

2 REGIONAL TECTONIC SETTING

With reported ages between 1.7 and 3.2 Ga, the Archean and early Proterozoic basement domains in Alberta have been suggested to deform and metamorphose more severely than the adjacent Superior, Wyoming, Slave and Nain provinces during the Palaeoproterozoic era (Burwash & Krupička 1969, 1970; Burwash & Culbert 1976; Hoffman 1988; Ross *et al.* 1991; Villeneuve *et al.* 1993). Interpretations of the regional tectonics heavily relied on aeromagnetic/potential field data, isotope age determination of drill core samples and extrapolation of tectonic elements from the exposed part of the Canadian Shield (Hoffman 1988; Villeneuve *et al.* 1993). Over 20 juxtaposed domains (Ross *et al.* 1991) have been identified in an oddly shaped region bounded by the Great Slave Lake Shear Zone, Snowbird Tectonic Zone (Snowbird TZ) and Vulcan structure, three tectonic discontinuities (Eaton *et al.* 1999a; Ross *et al.* 2000; Clowes *et al.* 2002; Banas *et al.* 2007) that potentially played major roles in establishing the regional tectonic framework. Among them, the Snowbird TZ divides the Archean hinterland of Trans-Hudson Orogen and has been widely recognized as a steep lateral gradient in gravity and magnetic field into the Hearne and Rae Provinces (Fig. 1; Hoffman 1988; Ross *et al.* 2000; Jones *et al.* 2002). This elongated structure is suggested to bifurcate around the Wabamun domain, a magnetic high bounded by narrow, south-

west striking magnetic and gravity lows (i.e. Thorsby and Rimbley domains). Reverse faulting (Ross *et al.* 1995), subduction and magmatism are probable causes of the isotopic composition of granitic rocks beneath the Snowbird TZ and its adjacent domains (Ross *et al.* 2000).

North of the Snowbird TZ, the most recognizable subdivisions from north-trending, convex-westward aeromagnetic signatures (Ross *et al.* 1991; Hammer *et al.* 1995a; Ross & Eaton 2002) and gravity observations are the Buffalo Head Terrane, Taltson Magmatic Zone and Rae Province (see Fig. 1; Ross *et al.* 1991; Villeneuve *et al.* 1993). Much of this region contains metaplutonic and subordinate felsic metavolcanic rocks with suggested ages of 2.0–2.32 Ga (Ross *et al.* 1991; Villeneuve *et al.* 1993), while the convergence of Slave and Rae provinces east of the Buffalo Head Terrane during the Palaeoproterozoic era (Thériault & Ross 1991; McNicoll *et al.* 2000) facilitated the development of the Taltson-Thelon Orogen, a north-trending magmatic belt comprised mainly of felsic and metasedimentary rocks. The segment sampled by this study is the southernmost section of this orogen, generally referred to as Taltson Magmatic Zone, which entails a 300-km-long section containing both Archean and Palaeoproterozoic metaplutonic gneisses but is distinctively younger than northwestern Alberta (McDonough *et al.* 2000; McNicoll *et al.* 2000).

Further east, the crustal signatures in central Alberta is a microcosm of the elaborate tectonic history of western North America. This region overlaps with southern Hearne province, a proposed Archean microcontinent as old as 2.8–3.5 Ga based on Zr and U-Pb analyses (Lewry & Sibbald 1980; Frost & Burwash 1986; Crocker *et al.* 1993; Bickford *et al.* 1994; Boerner *et al.* 2000). Despite an extensive history dating back to 3.0–3.5 Ga, much of the region may have undergone continental collision and intracontinental shortening during the early Proterozoic (1.7–1.9 Ga; Boerner *et al.* 1995; Edwards & Brown 1999; Ross & Eaton 2002). Recent tectonic models of the Hearne Province suggest coeval subductions along the Snowbird TZ in the west and Trans-Hudson Orogen in the east (Ross *et al.* 2000), centring on the Loverna Block—the largest subdivision of the Hearne province with a distinctive northeast striking aeromagnetic signature (see Fig. 1; Ross *et al.* 1991; Clowes *et al.* 2002). Much of the rocks beneath the Loverna Block are of Archean origin (Ross *et al.* 1991; Villeneuve *et al.* 1993), though evidence from geophysical and geochemical investigations has suggested extensive rework (Hoffman 1988; Ross & Eaton 1999; Boerner *et al.* 2000; Clowes *et al.* 2002; Gorman *et al.* 2002) and a potential clockwise rotation (Boerner *et al.* 1995). Also affected by these Proterozoic events are the surrounding domains such as Eyehill High, a 70-km-long positive aeromagnetic anomaly parallel to the Trans-Hudson Orogen (Hope & Eaton 2002), and an anomalously conductive (Boerner *et al.* 1995) Lacombe domain that borders with the Snowbird TZ. Despite evidence of weakly metamorphosed volcanic and sedimentary rocks, especially in the latter domain, the origin and seismic signatures of both domains remain speculative.

Southern Alberta mainly consists of the Vulcan Structure, an elongated domain with prominent east trending gravity and magnetic anomalies (Ross *et al.* 1991; Villeneuve *et al.* 1993), and the adjacent Medicine Hat Block that extends into northwestern United States. The Vulcan Structure spans more than 350 km longitudinally and cuts across the potential-field fabric of southern Alberta at a large angle (Eaton *et al.* 1999a, 2000). Drill core samples from this region suggest an early Proterozoic (circa 1.8–2.7 Ga) origin (Villeneuve *et al.* 1993), but the interpreted age and genesis differ considerably among the earlier studies (Eaton *et al.* 1999b; Lemieux *et al.* 2000). Equally controversial is the Medicine Hat Block, a

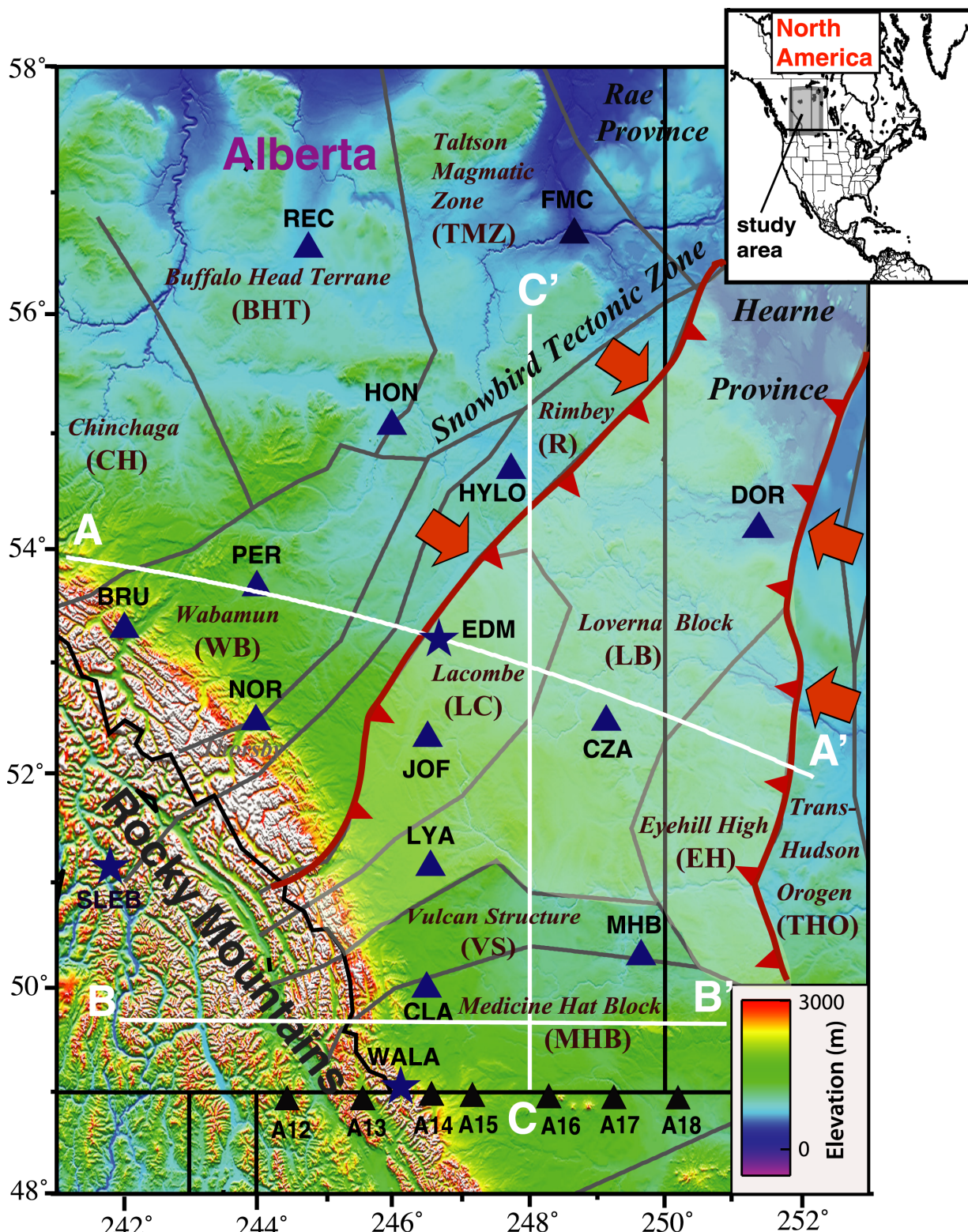


Figure 1. Distribution of broadband seismic stations from CRANE (blue triangles), CNSN (stars) and IRIS (black triangles). The background colours indicate the topographic relief of the region based on ETOPO2 database. The domain boundaries from Ross *et al.* (1991) and the great-circle surface projections of three cross-sections (results to be presented in Figs 12, 13 and Fig. S6) are denoted by grey and white lines, respectively. The Hearne craton is shaded in semi-transparent colours for emphasis, while the presumed subduction boundaries during the Proterozoic eon (Clowes *et al.* 2002) are highlighted in red color. The subducting plate and the direction of plate convergence are indicated by the arrows.

positive potential field anomaly flanked by the Archean Wyoming province (south of the study area) with granitoids as old as 3.2 Ga (Ross *et al.* 1991; Villeneuve *et al.* 1993). Layered lower crust and geometric cut-offs of the Medicine Hat Block are interpreted as the remnants of a complex geological framework (Lemieux *et al.* 2000); regional reflection profiling data favoured an origin in connection with the assembly of two ancient Archean blocks (Lemieux *et al.* 2000), whereas Proterozoic collisions between the Loverna Block and Archean Wyoming Province have been suggested as the dominant mechanism (Eaton *et al.* 1999b; Mueller *et al.* 2002). Post-collision injection of mafic melt has been traced to the base of the crust beneath the Medicine Hat Block, which potentially plays a key role in the crustal evolution of the adjacent Vulcan Structure (Lemieux *et al.* 2000; Mueller *et al.* 2002).

3 DATA AND METHODS

The data set analysed in this study consists of broadband recordings from 13 CRANE stations, 3 CNSN stations and 7 USArray stations (see Fig. 1). With an average spacing of ~ 150 km, CRANE provides the primary crustal constraint on Southwest WCSB whereas the inclusion of USArray, which operated in Montana during the limited time window from late 2007 to early 2009, is vital for a structural investigation of southern Alberta. Our first objective is to extract empirical Green's functions (e.g. Sabra *et al.* 2005; Shapiro *et al.* 2005) of the great-circle path between any two stations based on the correlation of ambient seismic noise (Gu *et al.* 2007, 2011; Bensen *et al.* 2008; Gu & Shen 2012); the average length of data for a given correlation stack is ~ 1.5 yr. The data preprocessing entails three steps: (1) segmenting

the piece-wise vertical component records into 12-hr intervals, (2) low pass filtering with a corner frequency of 1 Hz and (3) bit normalizing (Bensen *et al.* 2008) the filtered seismograms to minimize the effects of earthquakes and other high amplitude, non-ambient seismic signals. The overlapping time segments after pre-processing are cross-correlated and stacked to improve the signal-to-noise ratio (SNR), which is defined by the ratio of peak amplitudes of the signal (0–400 s) and noise (450–500 s) windows on stacked cross-correlation functions (SCCFs). While more than 300 SCCF are computed using the above approach, only 100–200 correlation stacks with $\text{SNR} > 2$ are eventually retained for each frequency range analysed in this study; this subjective cut-off value is chosen conservatively to ensure the quality of the travel time measurements. Fig. 2 shows all the SCCFs with acceptable SNR ratios for group velocity inversions. Under the ambient noise source assumption, SCCFs (and their derivatives) are effective Green's functions between two stations and their lag times reflect the associated seismic structure (Sabra *et al.* 2005; Shapiro *et al.* 2005; Yao *et al.* 2006). The peaks in the SCCF form semi-linear distance-time trends are, to first order, consistent with those of propagating Rayleigh waves (Gu *et al.* 2007, 2011; Bensen *et al.* 2008; Brzak *et al.* 2009). A sample SCCF from two CRANE stations (Fig. 3a) shows prominent noise correlation peaks that exhibit consistent positive and negative lag times relative to the origin. These peaks generally remain robust in a broad range of frequencies (Fig. 3b) and enable accurate determinations of effective Rayleigh wave group velocities (Shapiro *et al.* 2005; Lin *et al.* 2008; Ritzwoller *et al.* 2011; Kim *et al.* 2012). The residual effect of secondary non-ambient sources (Gu & Shen 2012), which is generally reflected in the slight asymmetry of the SCCFs (see Fig. 3b), is minimized by collapsing the positive and

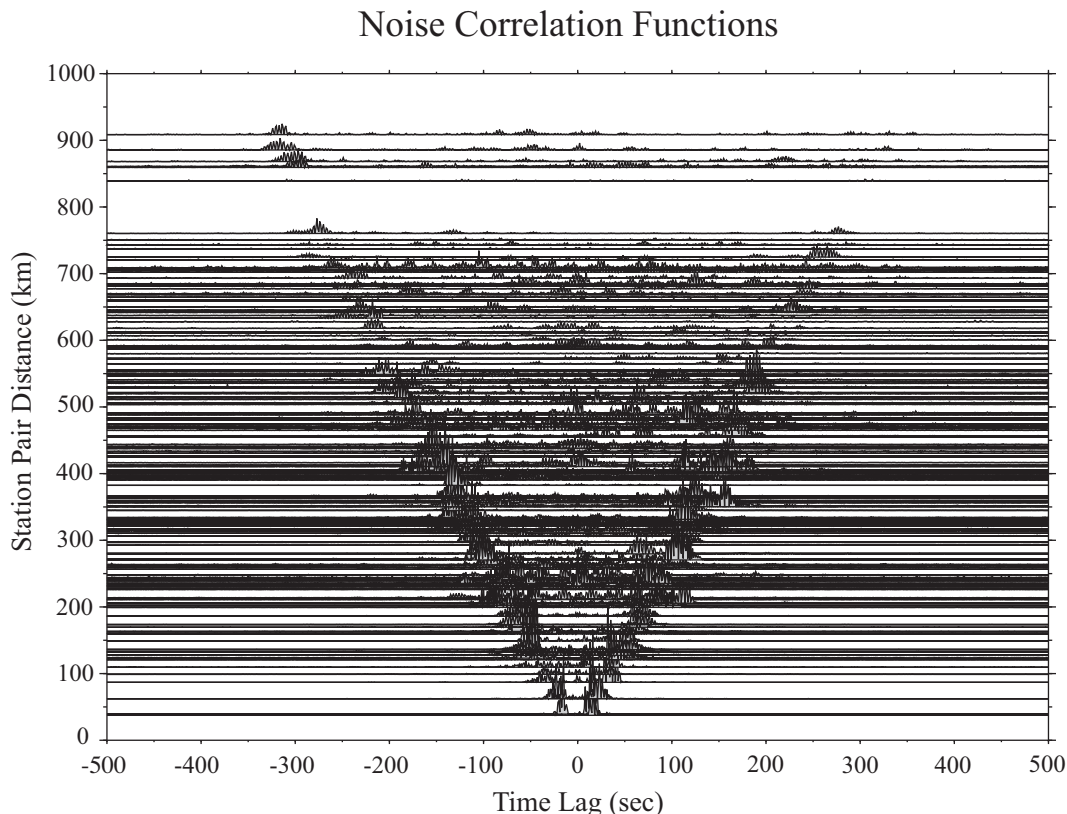


Figure 2. SCCFs computed for all station pairs with acceptable SNR. The arrival times of the SCCF peaks increase linearly at an approximate speed of 3 km s^{-1} .

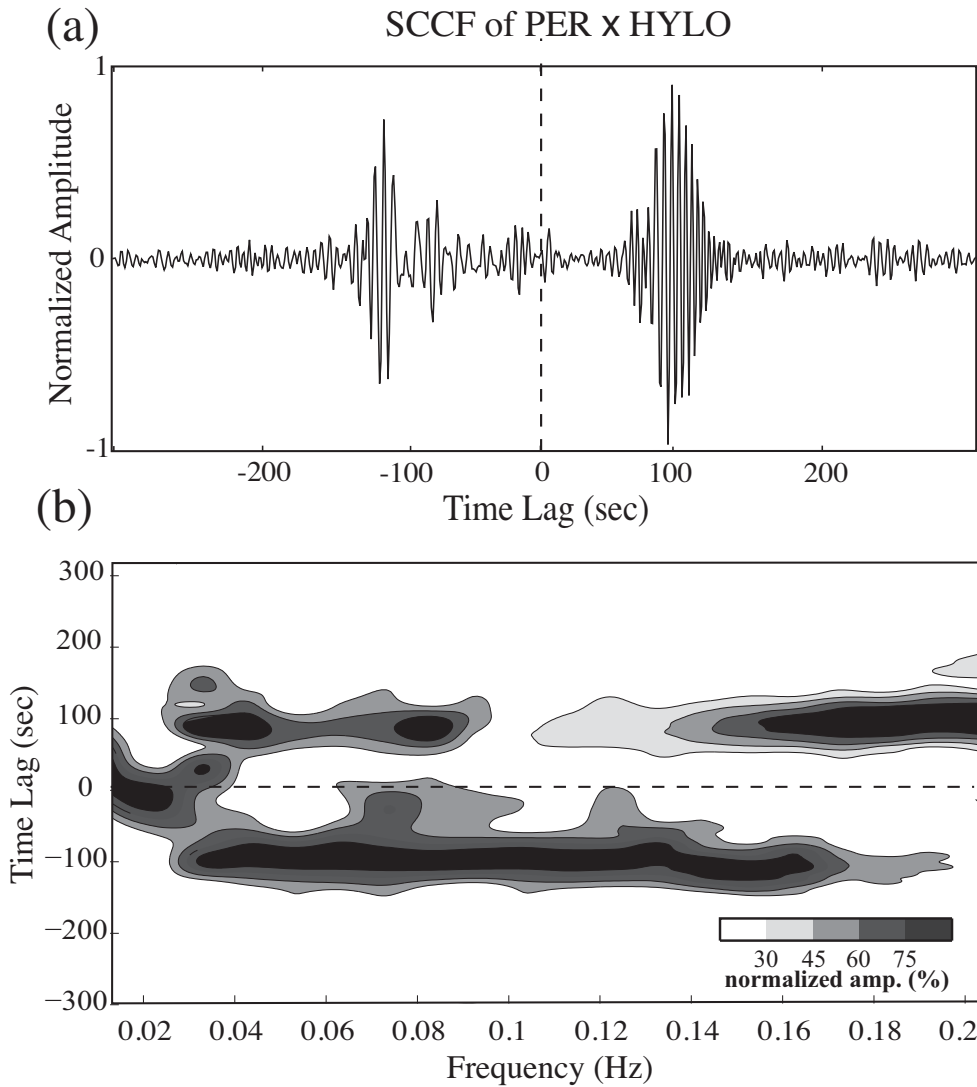


Figure 3. (a) Unfiltered SCCF between stations PER and HYLO. The average of forward and time-reversed SCCF peaks represents the effective Green's function of the path between the station pair. (b) Effective dispersion curves of the broadband SCCF within the frequency range of 0.015–0.25 Hz. The variable lag times of the correlation peaks demonstrate the effect of Rayleigh wave dispersion.

negative halves of SCCFs for effective average measures of lag times. To maximize data coverage we compute SCCFs for all possible combinations of stations. We then subject each broadband SCCF to a Multiple Filter analysis (Dziewonski *et al.* 1969; Dziewonski & Hales 1972; Herrmann 1987; Levshin *et al.* 1989) to determine the group velocity dispersion through a series of narrow (0.02 Hz in Gaussian Width) bandpass filters centred at every 0.02 Hz in the total range of 0.002–0.2 Hz (e.g. Cristiano *et al.* 2010); the bulk of the measurements are made within a realistically observable range of 0.016–0.2 Hz. Our implementation is similar to that of FTAN (Levshin *et al.* 1972; Levshin *et al.* 1989) and the choices of narrow bandpass filters and envelope speed measurements emphasize the fundamental mode surface waves (e.g. Schiavardi & Morelli 2009; Cristiano *et al.* 2010). For each passband we first compute the absolute values of the narrow-band SCCFs, and then construct an envelope function on the main phase group by fitting the local maxima of the individual peaks using a cubic polynomial. The peak of the envelope function, which is determined to an accuracy of 0.01 s, provides a frequency dependent constraint on the path structure between two stations. After a careful visual examination of all

group dispersion curves, we average the dispersion measurements within high quality passbands of 0.14–0.2 Hz, 0.1–0.16 Hz, 0.06–0.12 Hz, 0.03–0.08 Hz and 0.002–0.04 Hz. For simplicity we will refer to these five frequency ranges using the corresponding centre periods of 6, 8, 12, 23 and 40 s; the last centre period is an approximation based on the observed spectral amplitudes. The averaging is necessitated by the visible scatter in the narrow-band measurements, especially those in connection with temporary array stations residing on the soft glacial sediments of central Alberta.

We exclusively focus on group velocity measurements partly due to the larger-than-expected phase velocity variations in our region where signal quality is less than ideal. A more important consideration is the lack of source information and its negative impact on the accuracy of phase velocity determinations (e.g. Knopoff & Schwab 1968; Larson & Ekström 2001; Feng *et al.* 2004). For each frequency range, the automatically determined group arrival times for each station pair are then subjected to a linear distance–time analysis. The outliers, which are defined by velocity perturbations greater than 10 per cent of linear least-squares average velocities, are automatically rejected to improve the consistency of the

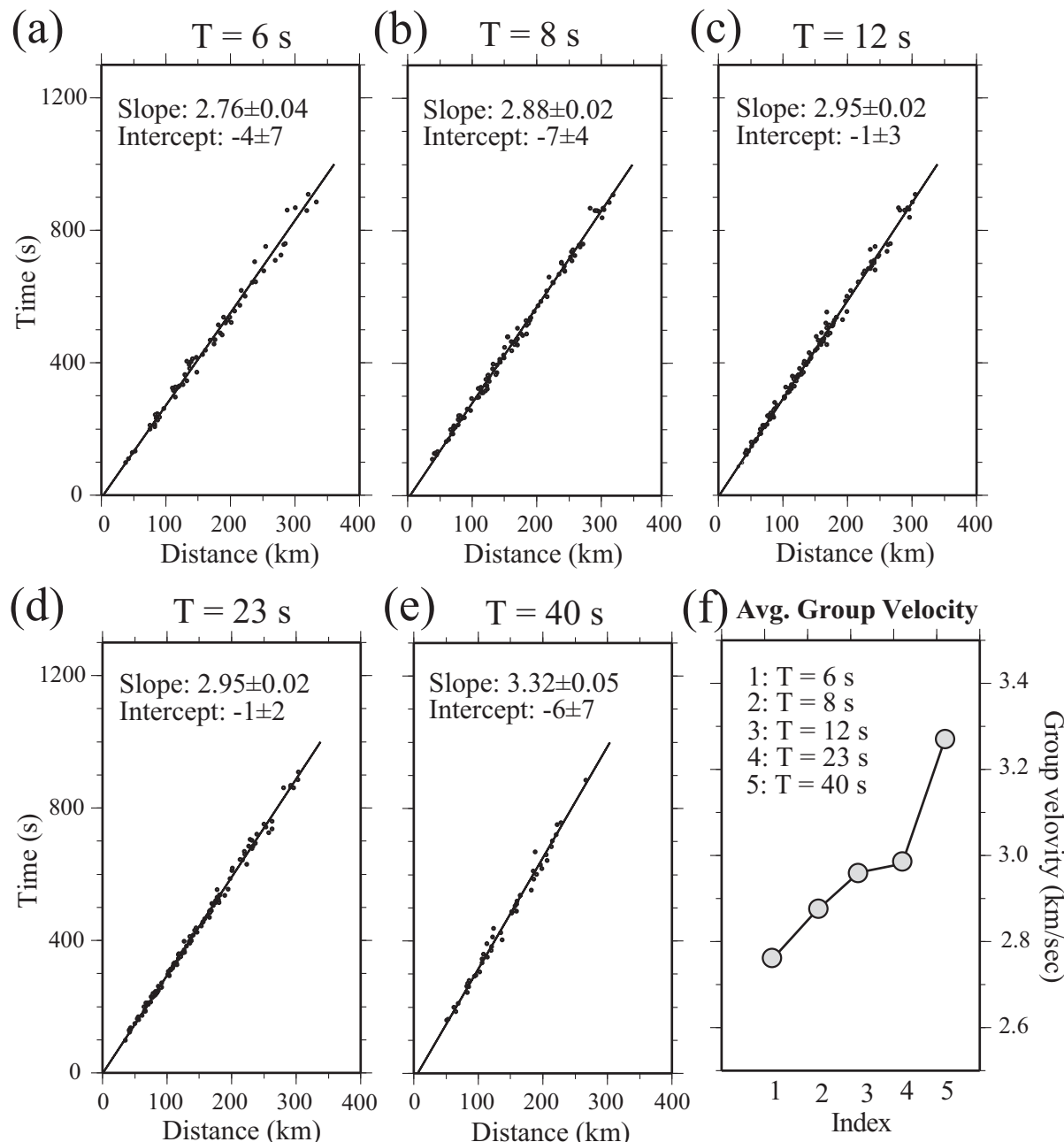


Figure 4. (a)–(e) Lag times of SCCF peaks for all five period ranges. The slopes of the least-squares linear fit (black lines) are the effective regional group velocity averages, while the intercepts can be used to gauge the uncertainties of the average velocities as well as potential biases in data quality and distribution. (f) A comparison of the average velocities. The trend indicates increasing average crustal speeds with depth.

measurements; this procedure eliminates 10–30 per cent of the raw measurements.

The peak arrival times of the envelope functions for all selected frequency ranges approximately follow linear move-out curves (Figs 4a–d) where the slopes of the best-fitting lines provide effective averages of surface wave group velocities. The distributions of the traveltimes residuals are approximately Gaussian with a standard deviation ranging between 2 and 3.5 s (Fig. S1). This value suggests an approximate data uncertainty of 3–4 per cent, assuming average inter-station distance and group velocity of 200 km (see Figs 4a–e) and 3 km s^{-1} , respectively. The intercept from linear regression is nonzero due to the presence of noise in the data, measurement

uncertainties and non-uniform data distribution. The magnitude of the intercept, which should be minimal at zero distance, is therefore a useful metric for data quality, that is, more reliable measurements are obtained for centre periods of 6, 12 and 23 s without considering the number of observations. The average group velocities of all period ranges fall between 2.8 and 3.3 km s^{-1} (Fig. 4f).

We subsequently perform nonlinear, 2-D tomographic inversions using the lag time measurements from the SCCFs. The inversion algorithm is based on the fast marching method from the fast marching surface tomography package (Rawlinson & Sambridge 2005) and performs 2-D ray tracing and subspace inversions. Successful applications of this method can be found in recent crustal

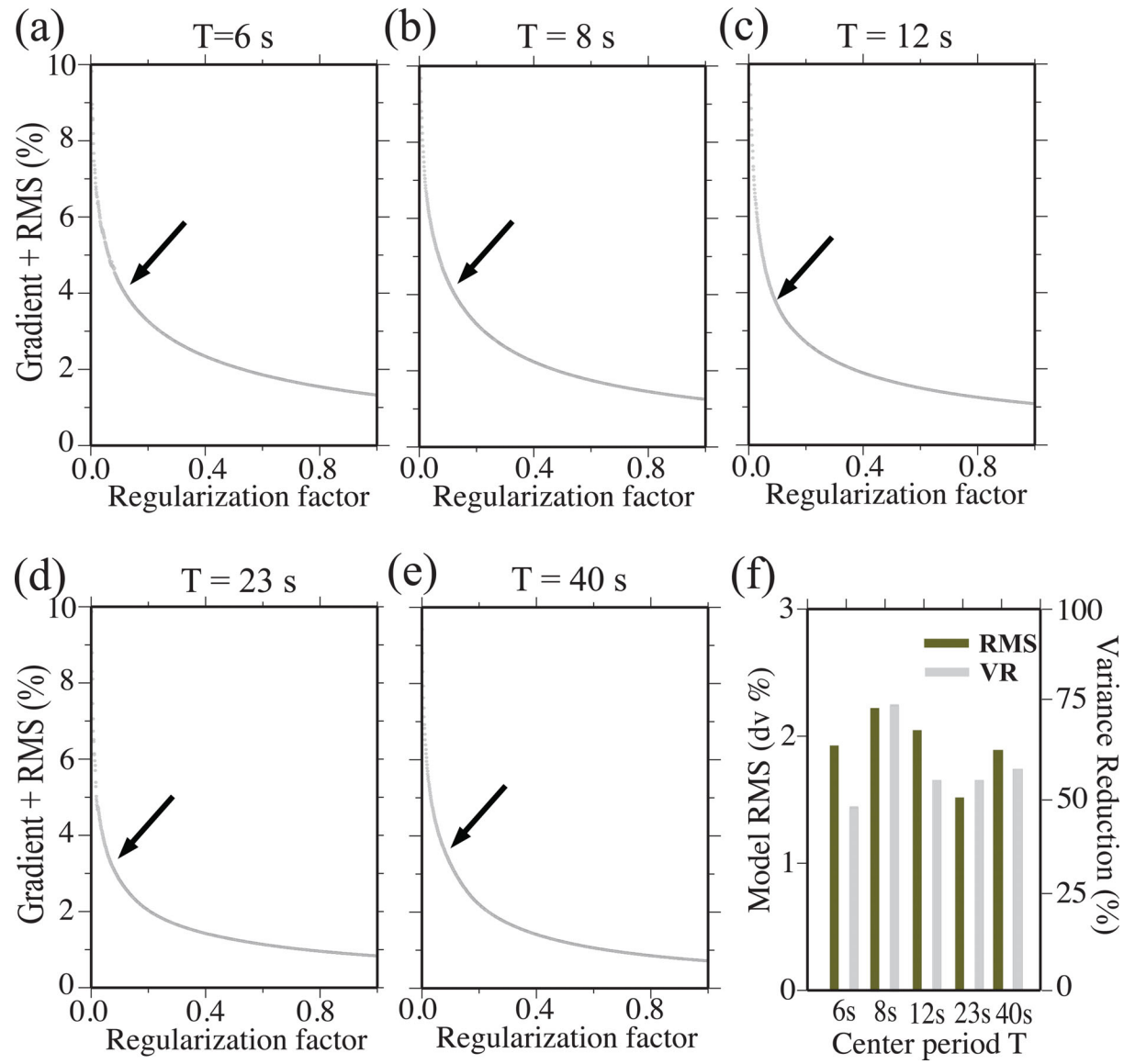


Figure 5. (a)–(e) Trade-off curves for the sum of norm+model gradients and model rms values. Equal weights are assigned to model size and gradient during the inversions. The optimal regularization factors for the inversions are determined by the turning points (denoted by the arrows). (f) Variance reduction (vertical scale on the right) and per cent rms model velocities (vertical scale on the left) at all period ranges. The Maximum model norm and variance reduction are both observed for the centre period of 8 s.

(Saygin & Kennett 2012) and mantle (Saygin & Kennett 2010) studies. To map the lag time measurements to velocities we first discretize the study region into $1^\circ \times 1^\circ$ (latitude \times longitude) cells, and then adopt the average group velocities (see Fig. 4f) as the 1-D reference model for 2-D inversions of lateral heterogeneities. The lag time measurements are subsequently inverted by updating both velocity and 2-D ray path (Rawlinson & Sambridge 2005). Measurements with residual-to-distance ratios greater than 0.25 s km^{-1} are eliminated during each iteration in well sampled regions to minimize the effect of outliers; slightly higher cut-off values are adopted for regions with limited path coverage. This reweighting procedure eliminates approximately 5–10 per cent of all measurements.

Due to the presence of noise and limited data constraints, solution to the inverse problem is highly non-unique and requires additional regularization measures. The inversions in this study aim to minimize the sum of variances in data residual, model size and model gradient. For each frequency range, the latter two terms in

the objective function are governed by the model norm and gradient damping parameters, respectively. Changes in the patterns of the model solutions are relatively minor for a broad range of damping parameters, while the amplitudes and gradients of seismic velocities systematically decrease with increasing regularization factors. We determine the optimal damping from the turning points of the trade-off curves with data fit (Rawlinson & Sambridge 2005). This is a subjective criterion that represents an effective compromise between data misfit and model attributes (e.g. smoothness, size; Gubbins 2004; Rawlinson & Sambridge 2005; Ammon *et al.* 2012; Aster *et al.* 2013). Values close to 0.05–0.1 are adopted as the norm damping parameters in the inversions of all frequencies (Figs 5a–e).

Reduction of data variance (for short, variance reduction) and root-mean-squared (rms) model coefficients for the frequency bands of interest are shown in Fig. 5(f). The former quantity is computed based on the residual lag times (data-model prediction) where data represent perturbations of path lag times relative to the reference

structure. The variance reduction used in this research is defined as

$$R = \left(1 - \sqrt{\frac{\sum_{i=1}^n (T_i^2 - T'_i)^2}{\sum_{i=1}^n T'^2}} \right) \times 100 \text{ per cent}, \quad (1)$$

where T_i and T'_i are the observed and model predicted lag times, respectively, for the i th station pair.

While fitting the absolute lag times between stations would yield variance reductions in excess of 90 per cent for all station pairs, variance reductions of lag-time perturbations (between 50 and 70 per cent) to the average velocities at each period range are more realistic estimations of the Green's functions between station pairs. Overall, the intermediate periods from 8 to 22 s are more confidently resolved than the two end frequencies. The values of the lateral group velocity variations range from 1.5 to 2.5 km s⁻¹. Shorter periods (below 12 s) show greater rms values than their long frequency counterparts, which suggest a relatively heterogeneous upper crust (see Section 5).

While the choices of regularization parameters during inversion are empirical (see Figs 5a–e) and somewhat subjective, the mean model residual variance of ~0.38 (1-VR in Fig. 5f) is roughly consistent with the observed data variance of 0.31 (Fig. S2). The compatibility between these two different measures of 'noise' in the data imposes, in the absences of truly unbiased estimates of data uncertainties and reliable 2-D regional velocity model, an independent physical constraint on the possible solutions of the inverse problem. A strong SNR within the primary ocean microseism period range of 8–10 s (Longuet-Higgins 1950; Gutenberg 1951), which is evident from the ratio between data and noise variances on the SCCFs (see Fig. S2), is particularly well explained by the inverted model with a residual variance less than 0.3.

4 2-D GROUP VELOCITY INVERSIONS

4.1 Assessment of data resolution

To quantify the data resolution we perform standard 'checkerboard' tests on all five frequency bands with an initial cell dimension of 1° (latitude) × 1° (longitude). A correction factor was introduced to account for the slight decrease in the actual cell sizes at larger latitudes (Rawlinson & Sambridge 2005). To simulate noise in the observations, we add a Gaussian-noise equivalent of 3 s, which is the average standard deviation of the group arrival times (see Fig. S1), to the simulated lag times prior to the inversions. The output models recover 60–65 per cent of the input model amplitudes for centre periods from 8 to 23 s (Figs 6a–c), as well as the general positions of model extremes. Velocity structures in central Alberta are especially well resolved, owing to the added high quality SCCFs in association with USArray stations. On the other hand, the northern part of the array (above 54° latitude) shows notable smearing effects due to reduced path coverage, particularly station REC near the northwestern corner of our study region owing to limited operation times between 2006 and 2007. The crustal velocities beneath the Rocky Mountains are better resolved than northern Alberta, despite fewer stations, due to higher quality measurements in association with CNSN station SLEB.

The two end-member period ranges are poorly resolved with grid sizes of 1 deg² due to limited path densities (Figs 6d and e). The minimum resolvable cell size for these periods is 1.5° × 1.5°, as suggested by more than 80 per cent recovery of the input amplitudes in southern central Alberta. Using the resolution tests as a guide, the

remainder of this section will emphasize group velocities beneath areas with sufficient resolutions south of 54° latitude.

4.2 Group velocity maps

Based on 6 s observations, ambient noise group velocities beneath central Alberta are ~6 per cent slower than those of the surrounding regions (Fig. 7a). The most conspicuous structure is an elongated low-velocity zone, which covers the length of the southern Loverna Block and eventually terminates in eastern Wabamun domain. The centre of this anomaly resides near the boundary zone between the Wabamun and Thorsby/Rimbey domains, which is surrounded by isolated high velocity centres beneath the Taltson Magmatic Zone (north), the foothills of the Rocky Mountains (west), as well as eastern Vulcan Structure and the Medicine Hat Block (south). Significant group velocity complexities, manifested in juxtaposed low and high velocities, are evident in the southernmost Alberta and the foreland belt of the Rocky Mountains.

The average group velocity increases from 2.76 to 2.84 km s⁻¹ at 8 s period. While high velocities remain roughly unchanged from the former passband (see Fig. 7a), a low-velocity zone east of the foothills in central Alberta (e.g. BRU and PER) becomes more prominent in size and amplitude (Fig. 7b). A north–south oriented, high velocity anomaly is observed near the border of Saskatchewan, segmenting the broad low-velocity zone from western Saskatchewan to central Alberta (see Fig. 7a). Combining with a high velocity zone within the foreland belt of the Rocky Mountains, this period range reiterates a major structural difference between central Alberta (slow) and the surrounding regions (fast). Furthermore, the western part of the Medicine Hat Block in the southernmost Alberta remains slower than the regional average despite a reduced east–west velocity gradient across it.

Significant high velocity zones are observed at 12 s along the foothills near the Alberta-British Columbia border, indicating below-average velocities in southern-central Alberta (Fig. 7c). On the other hand, apparent velocities beneath the Taltson/Buffalo Head terrane become ~5 per cent slower than the surrounding regions and continue southward by 100–200 km, which reinforce the low velocity zones in eastern Wabamun domain and central Loverna Block (see Fig. 7b). Similar structures are observed at 23 s period despite a visible loss of amplitude (Fig. 7d).

The seismic structures revealed by the longest periods (Fig. 7e) represent a major departure from those shown in Figs 7(a)–(d). The previously below-average Alberta Basin from shorter period maps is now occupied by a V-shaped high velocity zone that connects Medicine Hat Block with Wabamun domain and central Loverna Block. The maximum velocity beneath the latter region is ~10 per cent higher than the regional average of 3.3 km s⁻¹ and 20–25 per cent higher than those beneath the foothills of the Rocky Mountains. The northeast striking high-velocity zone below the Loverna Block, which is one of the most recognizable features from our group velocity inversions, is well resolved by the data. A consistent shape and over 75 per cent of the maximum input amplitude are accurately recovered by an inversion of simulated data based on a similar input structure with 3 s Gaussian noise (Fig. 8).

5 3-D SHEAR VELOCITY INVERSIONS

5.1 Procedures and model setup

Different frequency ranges investigated in this study provide sensitivities to different depths within the crust and/or shallow mantle

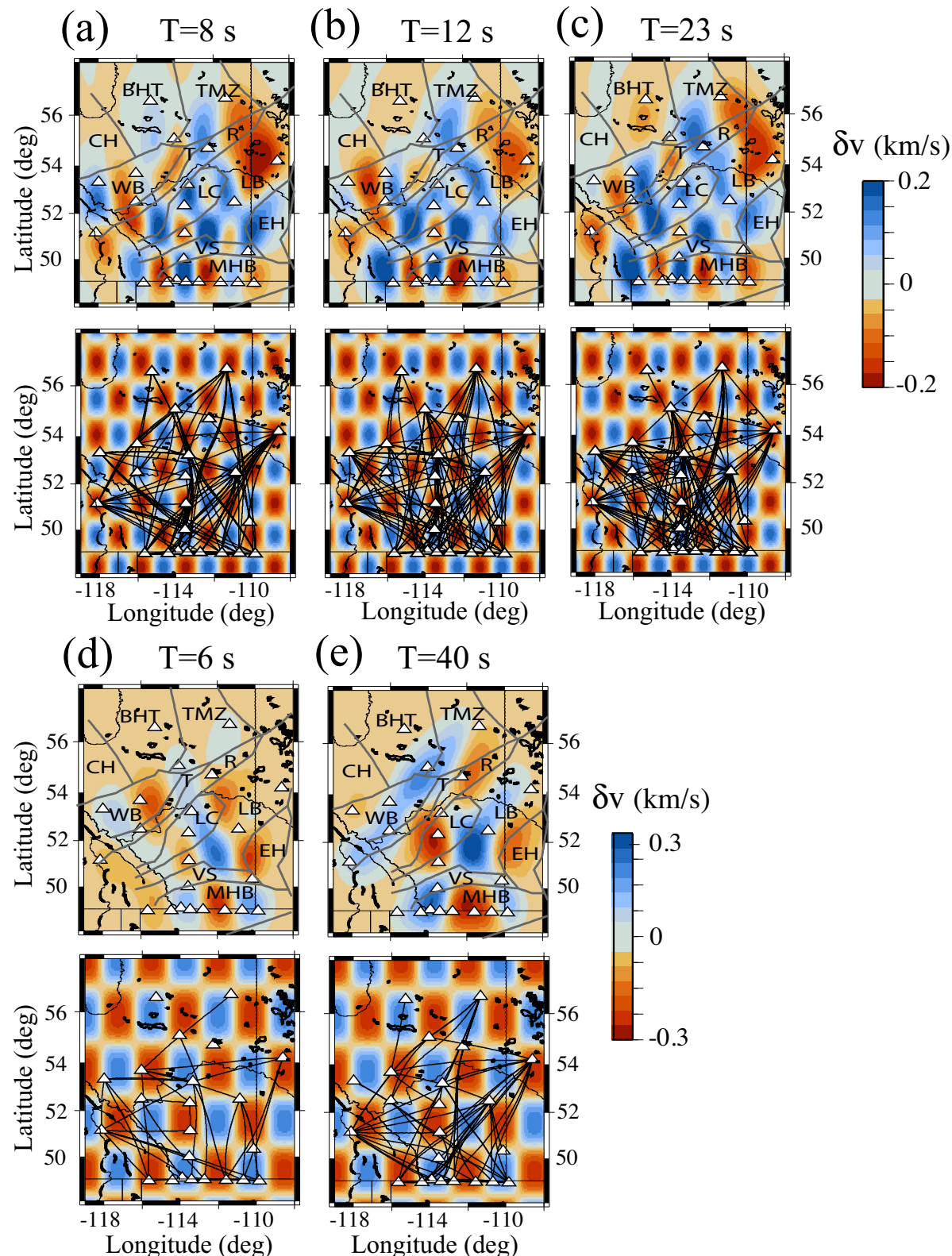


Figure 6. ‘Checkerboard’ resolution test for all five frequencies. The lower panels show the input checkerboard pattern with alternating positive and negative velocities of similar rms amplitudes to those of the actual velocities. The final SCCFs used for the inversion procedure are represented by the solid black lines connecting the available stations (white triangles). Gaussian noise with a half width of 3 s is added to the original model predicted times prior to the inversions. Bigger grid sizes ($1.5^\circ \times 1.5^\circ$) are used for centre periods of 6 and 40 s due to limited numbers of quality SCCFs. Approximated 60 per cent of the input amplitudes are recovered for the dense grids (a–c) and up to 90 per cent in the cases of coarser grid sizes (d and e).

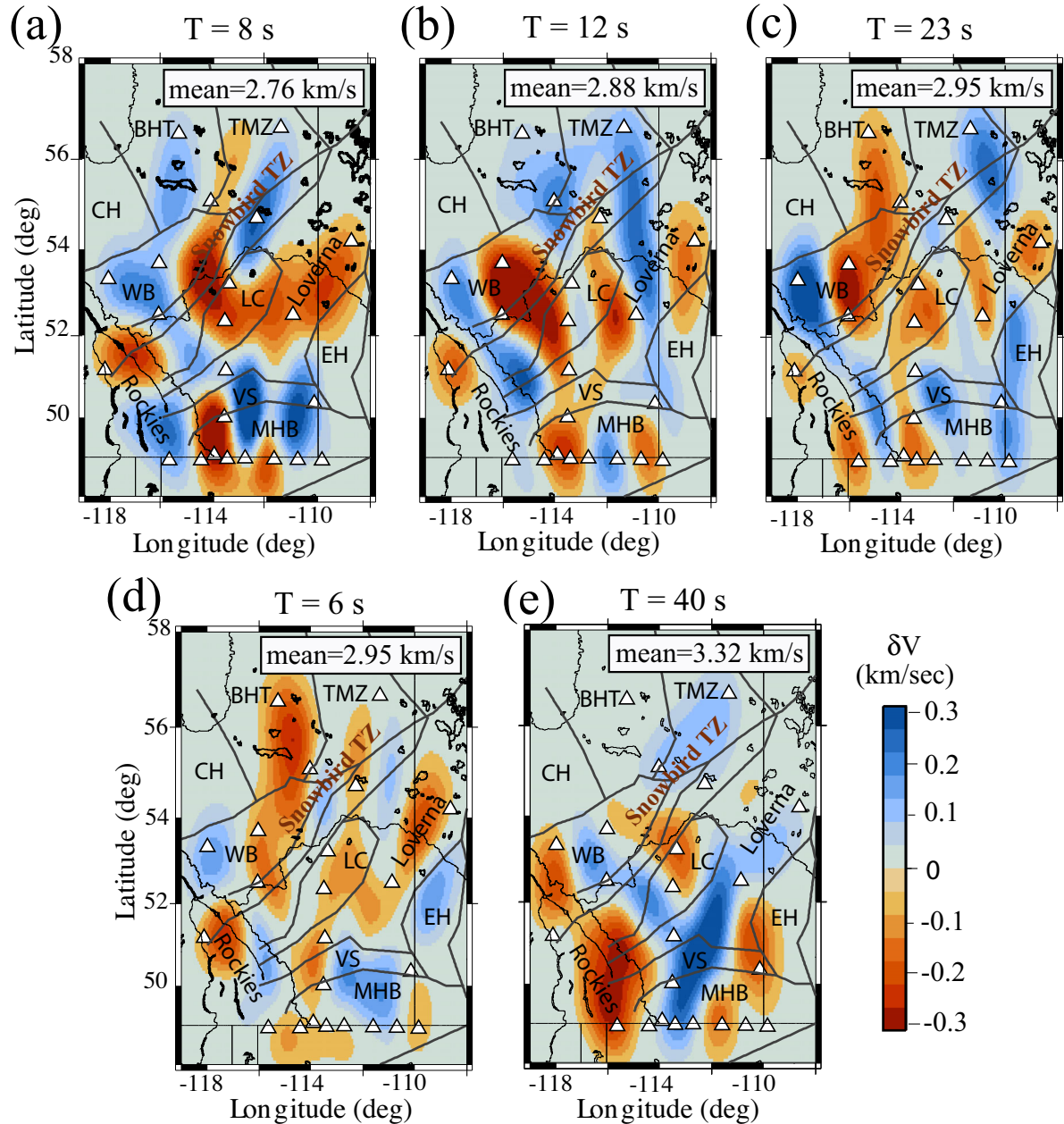


Figure 7. Results of the SCCF group velocity inversions. Velocities from each period range are plotted as perturbations to the regional mean values as indicated. The black lines denote the reported boundaries between the known tectonic blocks (Ross *et al.* 1991; see Fig. 1 for the definitions of the abbreviations). Stations used in this study are denoted by the white triangles.

(Fig. 9; Herrmann 2013). Centre periods from 6 to 23 s are primarily sensitive to shear velocities in the upper crust, as suggested by the peak locations of their sensitivity kernels, while the period range centring at 40 s provides the best constraints on the structure at depths below 30 km. Due to the apparent complexity of the sensitivity kernels (see Fig. 9), a proper assessment of shear velocities with depth would require a formal inversion of the group velocity dispersion results. To obtain 3-D shear velocities we compute model group velocity dispersion curves at 399 equally spaced nodes along the geographical coordinate system (latitude, longitude; Fig. 10a) based on the 2-D group velocity maps presented in Fig. 7. A 25-point linear interpolation is applied to the five group velocity measurements to stabilize shear velocity inversions for a 5-km-thick sedimentary layer (2 km of soft sediment overlying

3-km-thick shallow basement rocks) and 13 underlying layers with a uniform thickness of 5 km. For each location, a starting shear velocity model is obtained from recent inversions of receiver function data in the study area (Gu *et al.* 2011; Chen *et al.* 2015). The starting *P*-wave velocities, which impart less influence on Rayleigh wave group velocities than their *S*-wave counterpart, are scaled from *S* while assuming the materials of the crust and upper mantle are Poisson solids. The density structure is calculated from *Vp* using the Nafe-Drake relationship (Ludwig *et al.* 1970), while the ground anelastic effects are considered using values from PREM (Dziewonski & Anderson 1981).

The optimal 1-D shear velocities at each node location is obtained using an iterative linearized inversion method from Computer Programs in Seismology (Fig. S3; Herrmann 2013; Kao *et al.* 2013).

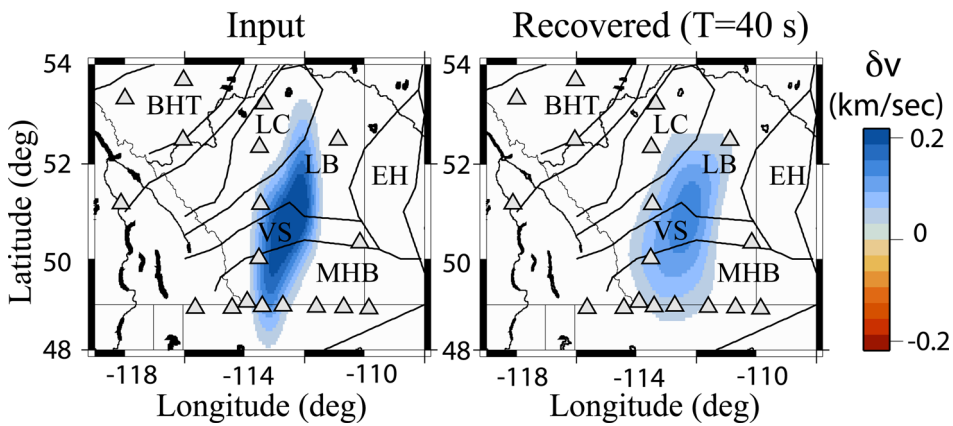


Figure 8. Results of a resolution test that assumes an input high velocity anomaly in southern-central Alberta. Simulated SCCF measurements between stations are obtained based on ray tracing. Both the amplitude and the oblique orientation of the input model are sufficiently recovered by the inversion for the centre period of 40 s.

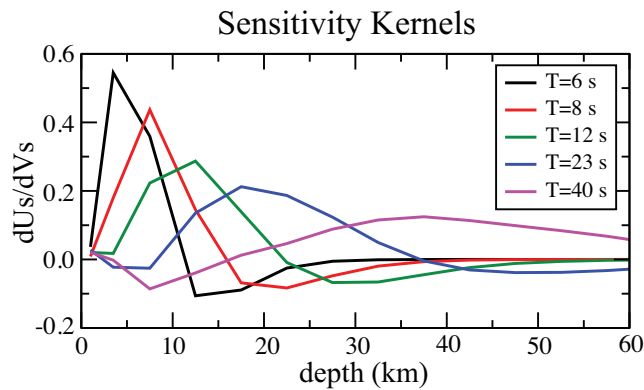


Figure 9. Sensitivities of group to shear velocities for the centre periods adopted in this study. The input 1-D model was obtained from a recent receiver function analysis of the study region (Chen *et al.* 2015). The peak sensitivities shift to greater depths at longer periods.

The regularization parameters (e.g. Aster *et al.* 2013), which aim to minimize both model norm and velocity gradients (see also Section 3), are determined for individual grid points based on the turning points on trade-off curves (Fig. 10b; e.g. Gubbins 2004; Rawlinson & Sambridge 2005). Our experiments show that the main features in the final inversion results are relatively stable over a wide range of regularization parameters, as well as for different choices of V_p and attenuation values. Most of the interpolated dispersion curves can be fit extremely well (Fig. 10c, examples P2–P4) except at a handful of grid points (see example P1, Fig. 10c). The variance reduction values for all grid points exceed 60 per cent, while the vast majority achieves a value over 90 per cent (Fig. 10d). Inherent smoothing during group velocity inversions (see Section 3) and the input of absolute group velocities (rather than perturbations) are largely responsible for the minimal misfit of the dispersion curves.

Our final 3-D shear velocity model is constructed via a simple spatial interpolation of the 1-D shear velocity models from all 399 gridpoints (Yang *et al.* 2012; Ward *et al.* 2013). The general strategy can be quantified as a two-step procedure that combines a 2-D group velocity inversion with a discretized 1-D shear velocity inversion. Similar approaches have been commonly adopted (Feng *et al.* 2004; Ward *et al.* 2013) and, in some cases, tend to reduce the nonlinearity of a direct 3-D inversion from group velocity measurements (Herrmann 2013).

5.2 Model assessment

The main purposes of the 3-D shear velocity inversion are to (1) verify robust features in the group velocity maps deduced from ambient noise correlation and (2) map the seismic velocities with depth. Our discussions will be limited to prominent shear velocity patterns in three broad depth regimes: (1) shallow crust, (2) middle crust and (3) lower crust. The choice of coarse layers and the inherent smoothing during the inversion procedures prohibit a definitive and accurate assessment of the sedimentary layer (1–2 km in the Alberta Plains), Moho as well as structures below 50 km.

The large-scale shear velocity structures in the shallow crust are strongly correlated with those from periods above 10 s (Fig. 11a) after the removal of regional averages at the corresponding depths. A strong velocity zone with three distinct centres is clearly visible beneath the Athabasca River Basin in the latitude range of 52–54°. Collectively, this anomaly spans nearly 600 km longitudinally, extending from eastern Hearne province to the Snowbird TZ. The maximum shear velocity centred near the Alberta-Saskatchewan border is approximately 15 per cent larger than the strengths of high velocities beneath eastern Vulcan Structure and the Medicine Hat Block in southern Alberta. The spatial correlation between this (see Fig. 11b) and the dominant low velocity structures from Figs 7(a–c) suggests strong depth sensitivities of all three passbands to the upper basement domains.

The structure in the middle crust (depth range of 11–25 km) is well represented in Fig. 11(b). The spatial scales of the structures generally decrease relative to those at shallower depths. Notable exceptions are the major low velocity zones beneath the Wabamun and Buffalo Head domains, which indicate a northward progression and strengthening of a similar structure in the shallow crust between the Lacombe and Wabamun domains (see Fig. 11a). A prominent low velocity structure is also observed beneath the foreland belt of the Rocky Mountains, which continues to the base of the crust (Fig. 11c). The overall pattern of heterogeneity in the middle crust shows little, if any, connection with the presumed domain structures.

Finally, the striking Y-shaped high velocity zone (see Figs 7 and 8) is easily recognizable in the depth range of 30–50 km (see Fig. 11c for a map at 38 km depth). There is a greater overall connection between lower crustal velocity and tectonic age/history than at shallower depths. In addition to a steep velocity gradient between the cratonic Loverna Block (fast) and the Rocky Mountain foreland belt (slow), which favours a deep-rooted craton-Cordillera transition, an argument could be made that the lower crust is considerably

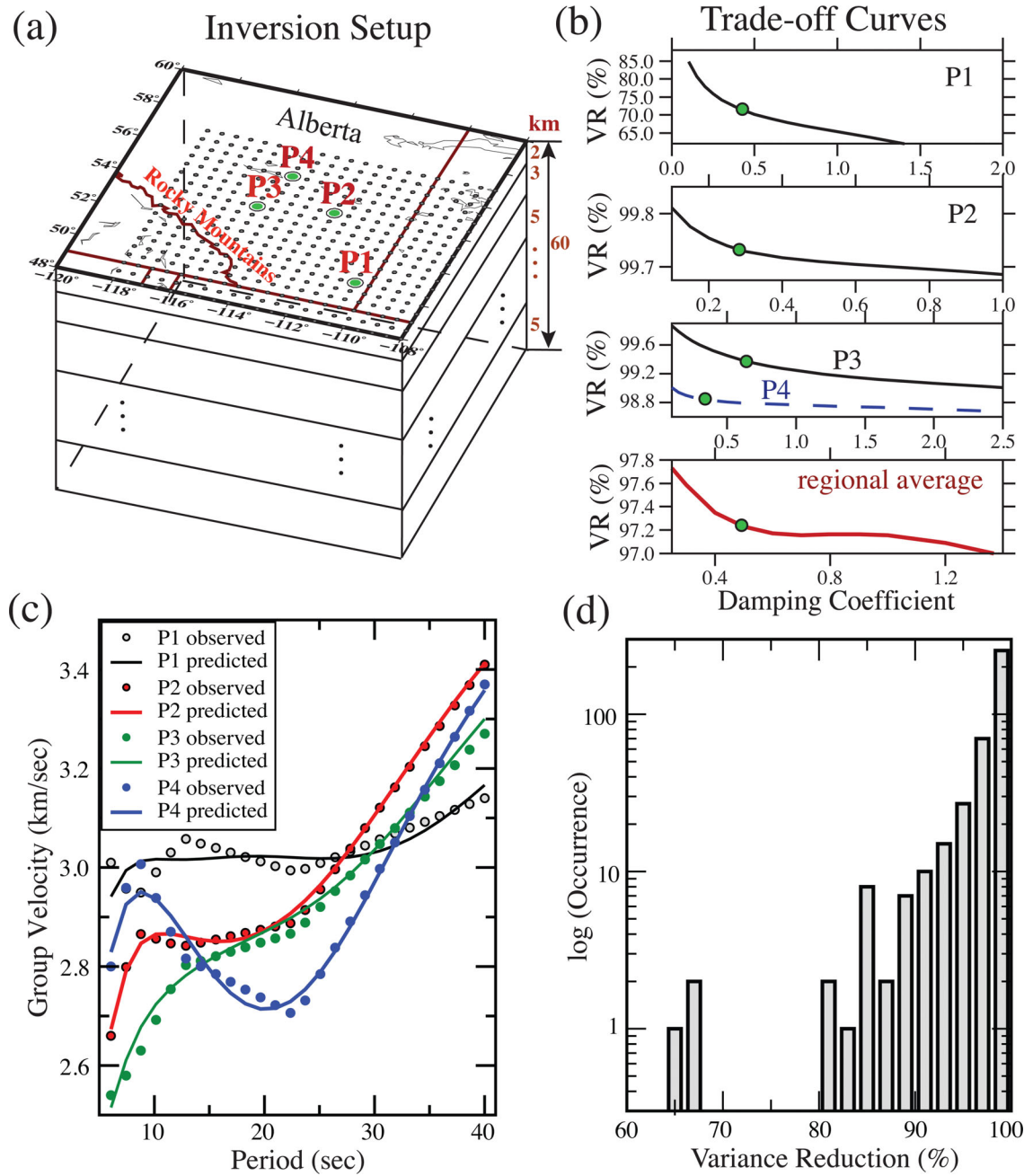


Figure 10. (a) Grid points (399, equal latitude–longitude spacing) and layer structures for the inversion of 3-D shear velocities. An iterative 1-D shear velocity inversion (Herrmann 2013) is performed on each node based on input group velocities from the five group velocity maps shown in Fig. 7. The model depths in the inversion range from 0 to 60 km. Two layers (with the respective thicknesses of 2 and 3 km) are adopted to represent the shallow sediment/basement structure, and the subsequent layer thicknesses are set at a constant value of 5 km. Four sample nodes (P1–P4) are selected to demonstrate the inversion procedure and outcomes. (b) Trade-offs between variance reduction and damping parameter for the four sample nodes shown in (a). The vertical axis corresponds to the percentage variance reduction. The green circles near the turning points of the trade-off curves denote the optimal values used in the inversion procedure. (c) Model fit to the input dispersion measurements for sample nodes P1–P4. At each node, a 25-point linear interpolation is applied to the five readings from the group velocity maps (see Fig. 7) prior to the inversion; an interpolation is needed to stabilize the inversion of 15 layer velocities. The coloured lines show the predicted dispersion curves from the 1-D shear velocity inversions at the four selected nodes. (d) Variance reduction of group velocity measurements (computed using a similar formulation as eq. 1) from all 399 nodes. Sample node P1 is selected in this demonstration due to its exceptionally small variance reduction value (<70 per cent).

faster beneath stable Archean and Proterozoic accreted domains (e.g. Hearne and Wabamun) than the presumed Proterozoic subduction zone (e.g. Snowbird TZ) and magmatic arcs (e.g. Talton Magmatic Zone).

The average 1-D crustal structure of the entire study region (Fig. 11d, red) is reasonably consistent with the existing results

from exploration seismic experiments (Fig. 11d, green; Bouzidi *et al.* 2002) and receiver function analyses (thick black line, Chen *et al.* 2015). The trend within the best resolved depths from this study (4–50 km) generally follow that of Bouzidi *et al.* (2002) after scaling P wave speeds under the assumption of a Poisson Earth. The most significant difference between these two models is a

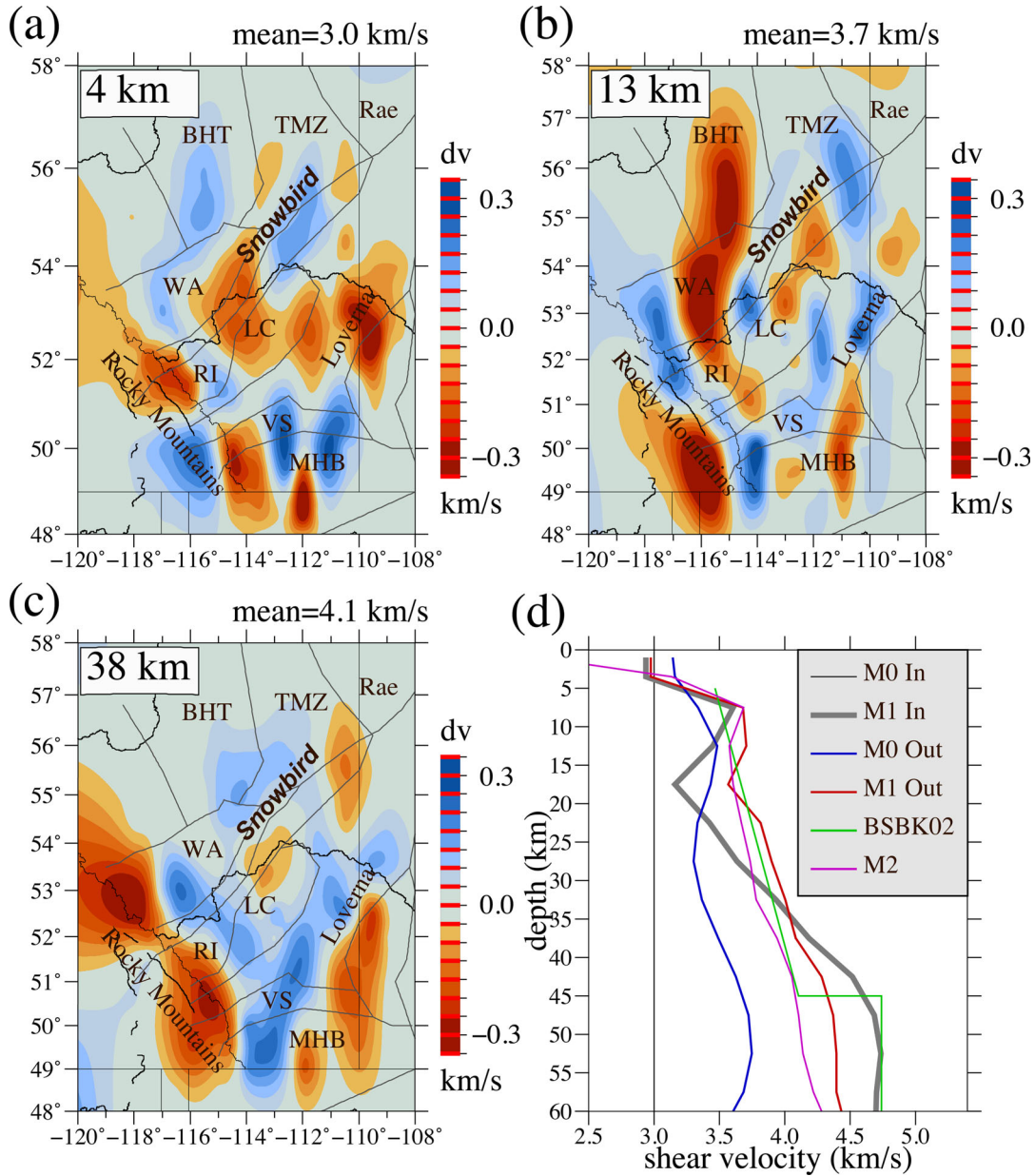


Figure 11. (a)–(c) Sample shear velocity perturbation maps. These maps are obtained by spatially interpolating the 1-D shear velocity structures from all 399 nodes (see Fig. 11a). The regional average at each depth, which are indicated on the figure, has been removed. The definition of domain abbreviations can be found in Fig. 1. (d) Model comparisons. The definitions of the model names are: M0 In (input model with a constant speed), M1 In [input model based on a regional study of receiver functions (Chen *et al.* 2015)], M0 Out (inverted shear velocity model based on input model ‘M0 In’), M1 Out (inverted shear velocity model based on input model ‘M1 In’), BSBK02 (scaled 1-D shear velocity model of Bouzidi *et al.* 2002), and M2 (an inverted model based on laterally varying input 1-D structures). The details of the last model are presented in the caption of Fig. S5. The output models of this study are obtained by averaging all 399 inverted 1-D models (see Fig. 10a for the corresponding node locations). The P-to-S scaling factor (1.732) for BSBK02 is based on the assumption of a Poisson solid.

distinctive low velocity zone between the depths of 12–20 km from our dispersion analysis. The same feature is present in the starting model (see Chen *et al.* 2015), though the size and strength of the low velocity structure differ considerably between our regional average and the input model. Part of discrepancies between input and inverted models can be attributed to differences in averaging area, as Chen *et al.* (2015) samples only central Alberta where the low velocity zone structure is the most prominent.

The choice of starting model has considerable influences on the outcomes of the inversions (e.g. Rawlinson & Sambridge 2005). To examine the stability of the inversion results we perform an inversion

using a constant 1-D starting model of 3 km s^{-1} (see Fig. 11d). The resulting regional average approaches the final solution (see Fig. 11d, red), both in terms of the general shear velocity pattern (Fig. S4) and in a low velocity middle crust (see Fig. 11d). However, the absolute values of the velocities and the suggested depths/widths of the low velocity zones clearly depart from our final solution. A similar conclusion is reached when the input model vary laterally according to Chen *et al.* (2015; see Fig. 11d, purple; Fig. S5). In all test cases key lateral shear velocity variations (e.g. the presence of a low-velocity structure in the upper crust) are well resolved, but the absolute velocity at a given depth is strongly dependent on the

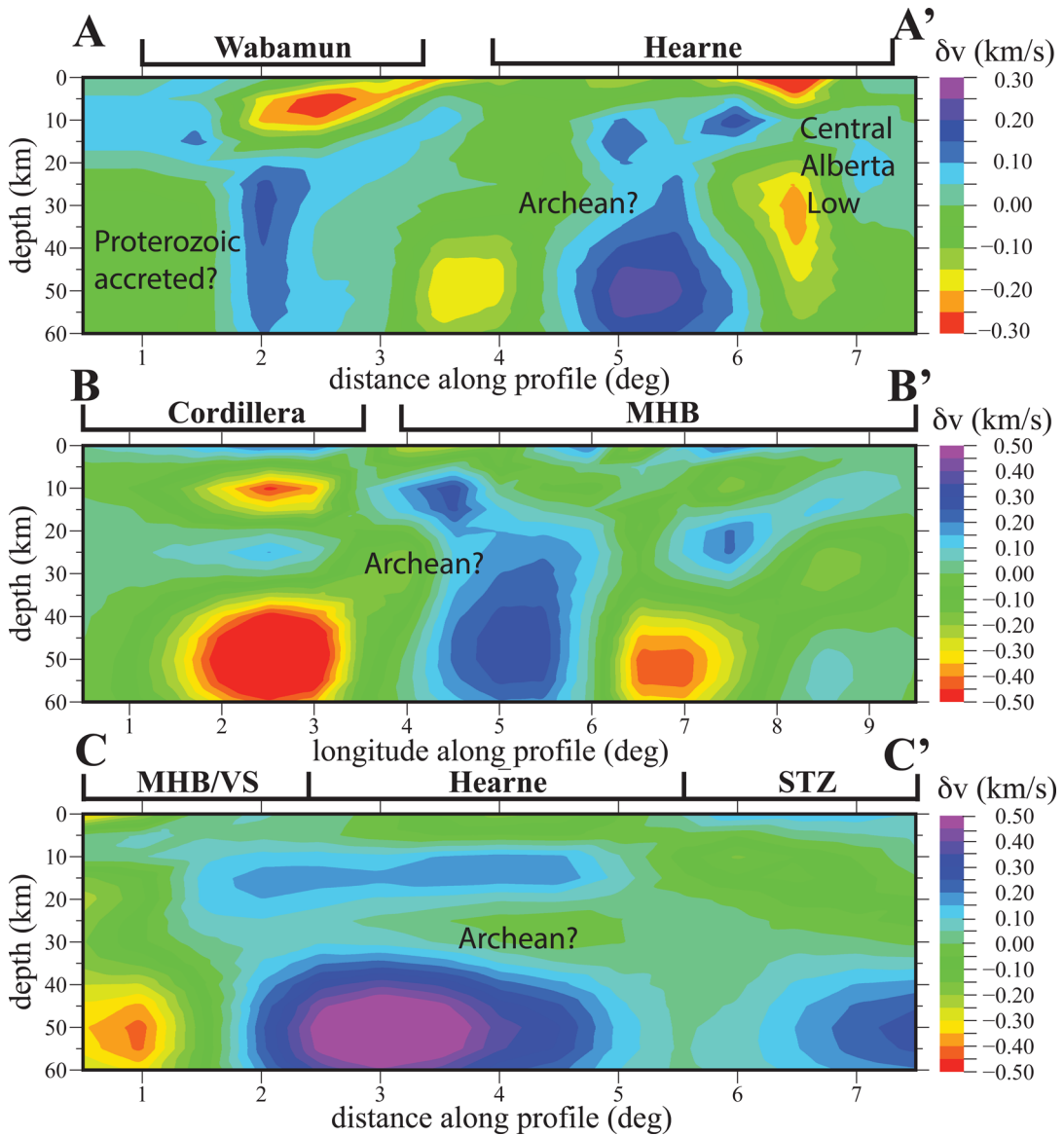


Figure 12. Cross-sections (see Fig. 1 for the corresponding surface projections) of the 3-D shear velocity model from this study. Key features and their potential implications are labelled. The cross-sections have been smoothed using a bi-linear algorithm (Wessel & Smith 1998) and the average velocity at each depth (i.e. model ‘M1 Out’ in Fig. 11d) has been removed.

a priori input model. In other words, caution has to be exercised when interpreting the average 1-D model structures from this study.

Sample cross-sections of our model reiterate the main observations from the shear velocity maps (Fig. 12). First, the northeast-oriented high velocity structure is well captured in all three cross-sections, partly owing to its substantial along-strike dimension. Depending on the viewing angle, this anomaly could potentially reach the upper crust. Also present is a vertical high velocity zone beneath the Wabamun domain, rivaling the broader anomaly beneath the Hearne craton in a semi east–west oriented cross-section (Fig. 12a). The shear velocities above and around this twin structure are generally below the regional averages, especially at shallow crustal depths. Beneath the southernmost Alberta (Fig. 12b), the lower crustal velocities are best characterized by strong gradients from the foreland belt of the Rocky Mountains to the Alberta plains. A secondary low velocity zone is also present beneath eastern Medicine Hat Block, which is easily recognizable in both cross-sections BB' (see Fig. 12b) and CC' (Fig. 12c).

To assess depth resolution we compute theoretical dispersion curves from (1) a modified regional average 1-D model from Chen *et al.* (2015) and (2) a constant 1-D model, add 4 per cent Gaussian noise (roughly equivalent to 0.12 km s^{-1} in absolute values) at each period, and perform shear velocity inversions using the same data sets and regularization parameters specified in Sections 2 and 3. The choice of noise level is made based on the standard deviation of the time measurements (<4 per cent; see Fig. S1) while assuming an average shear velocity of 3 km s^{-1} at all depths. For the same cross-sections in Fig. 12, the recovered model based on a realistic regional model containing a low velocity crustal layer (see Fig. 11d, Model M1 In) shows significant departures from the input at depths above 3 km and below 50 km (Fig. 13). This zonal pattern result from combined effects of (1) poor depth sensitivities of the five period ranges outside 5–45 km range, and (2) smoothing at the boundary depths with minimum (<2 km s^{-1} above 2 km depth) and maximum (>4.2 km s^{-1} below 50 km depth) input velocities. Aside from a relatively well-resolved depth range of 10–40 km (with

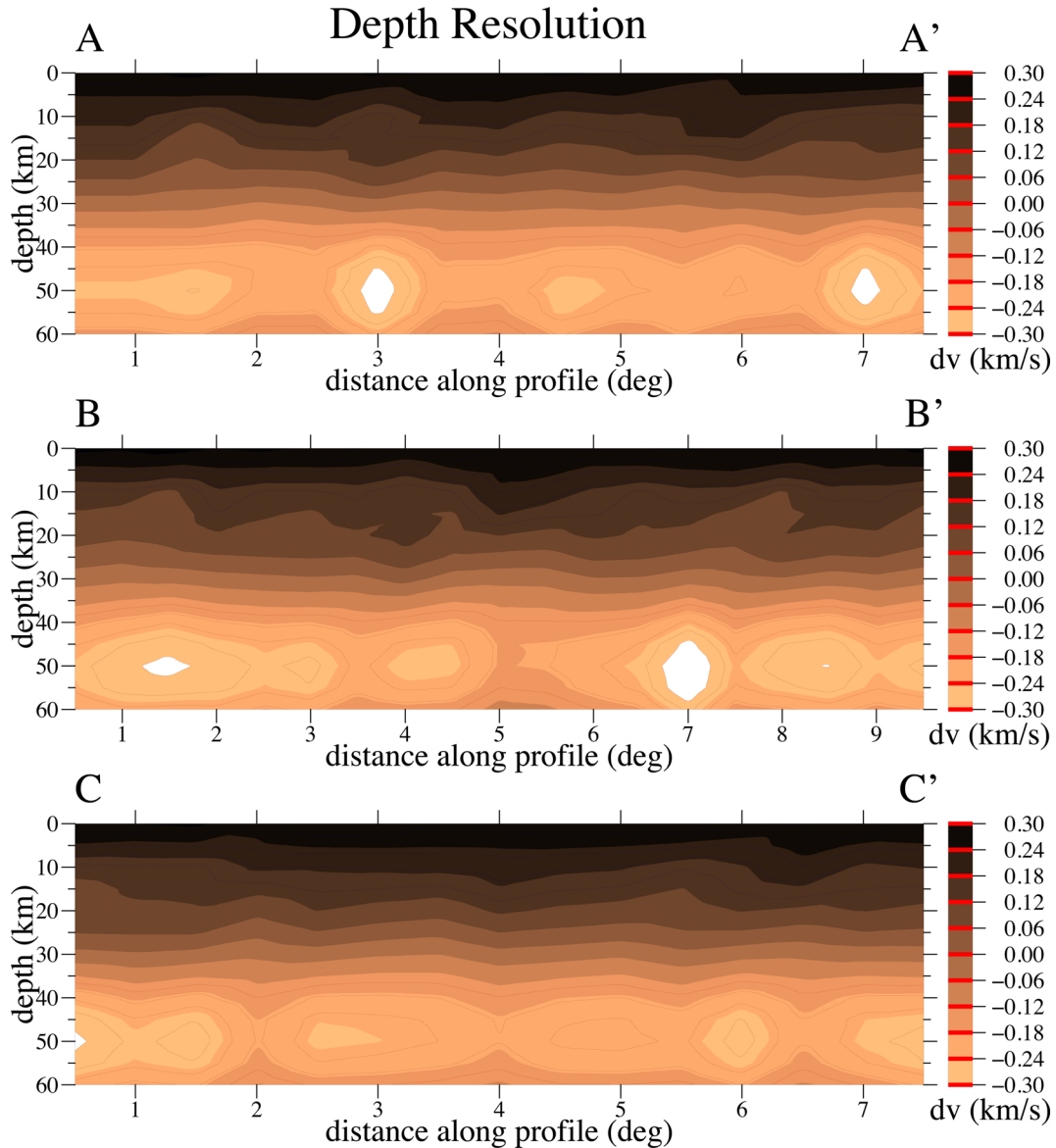


Figure 13. The same cross-sections as Fig. 12, but for an inverted model from a vertical resolution test. Theoretical dispersion curves are computed using “model ‘M1 In’” (see Fig. 11d), with an additional 4 per cent Gaussian error (equivalent to 0.12 km s^{-1}) prior to the inversion. The regularization parameters are the same as those in the actual inversions. The velocities shown in this figure are the interpolated differences between input and output models at each node, which show a zonal pattern and large model differences at depths above 5 km and below 40 km. The reduced resolution away from mid crust is a combined function of the *a priori* model (see Fig. 11), group velocity frequency–depth sensitivity (see Fig. 9) and regularization (see Fig. 10).

uncertainties below 0.1 km s^{-1}), it is encouraging that most of the key observations (low velocity zones beneath central Alberta basin and Cordillera, high velocities beneath the Wabamun domain and Loverna Block) do not overlap with the extrema in model uncertainty (e.g. near 7 and/or 3° along profiles AA' and BB'). Similar results are obtained for the case of a constant input 1-D velocity, though the lack of a zonal pattern and smaller overall uncertainties (Fig. S6) are further evidence for the non-negligible effect of *a priori* 1-D velocity structures.

6 DISCUSSION

The main objective of this study is to improve our knowledge of the crustal structure and history beneath Southwest WCSB, a region critical for the understanding of the formation and tectonic development of western Laurentia. The broadband ambient noise

SCCFs documented in this study offer detailed seismological constraints on the crustal and shallow lithosphere beneath the study region. We find that the average group velocities increase at longer periods, as are expected from the dispersion of Rayleigh waves, while strong gradients in the patterns of lateral heterogeneities and depths suggest possible variations in regional crustal temperature, lithology and composition (Barton 1986; Christensen & Mooney 1995; Jaupart *et al.* 1998; Brocher 2005; Jones *et al.* 2005).

6.1 East Alberta Orogen and the Snowbird TZ

Group velocity structures south of the Snowbird TZ are generally well resolved and offer some of the most revealing observations pertaining to the crustal formation of the study region. One persistent observation from the tomographic inversions of SCCFs is a bifurcated crustal structure within the proposed Wabamun domain.

According to Figs 7 and 12, the western half of the domain near the foothills of the Rocky Mountains is distinctively faster than the southeastern sectors in the upper crust but the trend reverses in the lower crust. A major east–west gradient in velocity highlights a possible crustal structural boundary between the Wabamun domain, an aeromagnetic high (Ross *et al.* 1991) featuring a west-trending low velocity zone (Zelt & Ellis 1989; Eaton *et al.* 1999a; Ross *et al.* 2000), and a contrasting Chinchaga domain/Rocky Mountain foreland belt with low magnetic susceptibilities (Ross *et al.* 1991; Villeneuve *et al.* 1993). If this velocity gradient marks the true domain boundary, then the Wabamun-to-Chinchaga/Rockies transition should be less continuous than that suggested by earlier reports based on active source seismic lines (Ross & Eaton 2002). In other words, the structurally coherent part of the Wabamun domain is at least 20–30 per cent smaller than the existing domain boundaries (e.g. Ross *et al.* 1991).

Noise correlation tomography sheds further lights on the preservation of the Snowbird TZ in central Alberta. As a highly controversial geological structure across the vast landmasses of Canada, the origin of the Snowbird TZ has been widely associated with collisions between the Rae and Hearne provinces nearly 1.9 Ga ago (Berman & Bostock 1997). The details of the tectonic events and their aftermaths remain speculative, primarily pertaining to the proposed mechanisms involving shear deformation at ~ 2.6 Ga (Hanmer *et al.* 1995a), subduction during the Proterozoic (Ross *et al.* 1991; Eaton & Cassidy 1996), and incipient rifting on an old, 2.5 Ga orogenic belt (Flowers *et al.* 2006). The shear velocity inversion results from this study show little, if any, definitive evidence for the presence of the Snowbird TZ in the upper crust. Widespread low velocities are generally observed in central Alberta, covering much of the Thorsby and Rimley domains, and the lineation of structural joints are much more complex than the expected northeast–southwest orientations at shallow crustal depths. The lateral dimension of the low velocity zone suggests diminished upper crustal variations across the Snowbird TZ (Ross *et al.* 1991; Villeneuve *et al.* 1993; Hanmer *et al.* 1995a; Flowers *et al.* 2006; Berman *et al.* 2007). The lack of distinctive signatures surrounding this suggested geological boundary may be partially explained by the presence of a mid-crustal low velocity zone (see Fig. 11d) in the 1-D regional average, which is especially significant in central Alberta. If the Snowbird TZ is of collisional origin in connection with the East Alberta Orogen (Ross *et al.* 1995; Berman *et al.* 2007) and coeval subduction during the development of a Proterozoic tectonic vise (Eaton *et al.* 1999a; Ross *et al.* 2000), then extensive crustal metasomatism, thickening and possible serpentinization (Eaton & Cassidy 1996) of oceanic lithosphere (see Fig. 1) should be expected during the Palaeoproterozoic era. Consequently, widespread partial melt from the base of the crust could significantly alter the composition of the upper crust (e.g. becoming more granite and granulite rich) and thereby obscure the delineation of structural boundaries and domains (see Figs 1 and 11; Chen *et al.* 2015). In other words, aside from the compelling evidence of widespread magmatic/granite intrusions, the Proterozoic signatures in Southwest WCSB are nearly beyond recognition within the upper crust (e.g. see Figs 11 and 12).

6.2 Hearne craton and southern Alberta

The seismic structure in the lowermost crust and shallow mantle are largely dominated by a Y-shaped high-velocity anomaly beneath the Loverna Block as well as the Vulcan Structure and Wabamun domain (see Figs 7, 8, 11 and 12). The presence of this anomalous

crustal signature has not been previously reported and warrants a closer examination in the context of regional tectonics. One of the key considerations is the role of the Hearne province, which formed during the late Archean but underwent major Proterozoic reworking. It has been hypothesized that its Palaeoproterozoic convergence with the Wabamun domain and the Trans-Hudson orogen gave rise to a collisional plateau between the dual subduction zones (e.g. Ross 2000). The fate and state of the Hearne lithosphere remain debated (Aspler *et al.* 2002; Shragge *et al.* 2002), though it has been suggested that the thickened lithosphere became gravitationally unstable and eventually delaminated from the base of the Loverna Block (Clowes *et al.* 2002).

The observed high velocity anomaly near the base of the crust is unlikely to be directly related to the subducted Proterozoic slabs, as significant thermal signatures relevant to that timescale (>1 Ga) should have long been eliminated. Instead, the unique orientation (northeast striking) and substantial strength of the observed high-velocity structure are better explained by relic, potentially undeformed, part of the Archean Hearne province (Boerner *et al.* 2000). The accompanying high velocity, lower crustal structure beneath the Wabamun domain (see Figs 12 and 13), a Precambrian craton with a Proterozoic accretionary origin, is further evidence for the overall preservation of Precambrian structures in the lower crust.

The presence of relic Archean crust in southern-central Alberta has further implications for the tectonic evolution of Southwest WCSB. A region of interest is the Vulcan Structure, a proposed tectonic boundary between the Loverna Block and the Medicine Hat Block with suggested origins such as a failed Proterozoic rift (Kanasewich *et al.* 1969) and a large magmatic Proterozoic suture (Thomas *et al.* 1987) between these two geological domains. Based on shear velocity inversions, Vulcan Structure is nearly indistinguishable from the Loverna Block in the lower crust where a pronounced high velocity, lower crustal layer (from here on, HLCL) continues across western Medicine Hat Block along a northeast–southwest orientation. The orientation, strength and continuity of this structure collectively favour a southward extension of the undeformed core of the Archean Hearne province. Still, the origin of the Vulcan Structure, a proposed deformation complex, remains debatable due to earlier findings of its signature and confinement within the top 20–30 km of the crust (Clowes *et al.* 2002). The velocity reversal from upper to lower crust beneath the Vulcan Structure (see Fig. 11) suggests distinct crustal history and/or composition with depth.

It is noteworthy that the boundary between the Vulcan Structure and the Medicine Hat Block is poorly defined by the inverted crustal velocities, in spite of earlier reports of older rock samples from *ca.* 3.2 Ga (Villeneuve *et al.* 1993; Gorman *et al.* 2002) from the latter domain. Lemieux *et al.* (2000) proposed that the Medicine Hat Block was the suture zone during the amalgamation of the more ancient Hearne and Wyoming cratons in the middle Archean (*ca.* 2.6 Ga; Mueller *et al.* 2002). This finding propelled the earlier hypothesis that Medicine Hat Block was originally a part of the Archean Wyoming province (Boerner *et al.* 1998; Henstock *et al.* 1998; Clowes *et al.* 2002). Our tomographic imaging results show that the lower crustal/upper mantle velocities beneath this region are comparable to those beneath the southern Loverna Block and Vulcan Structure, two adjacent domains dominated by Archean HLCL signatures. Barring resolution issues, the strength and continuity of the HLCL suggest that northwestern Medicine Hat Block was potentially an integral part of, or had been strongly influenced by, the Hearne province.

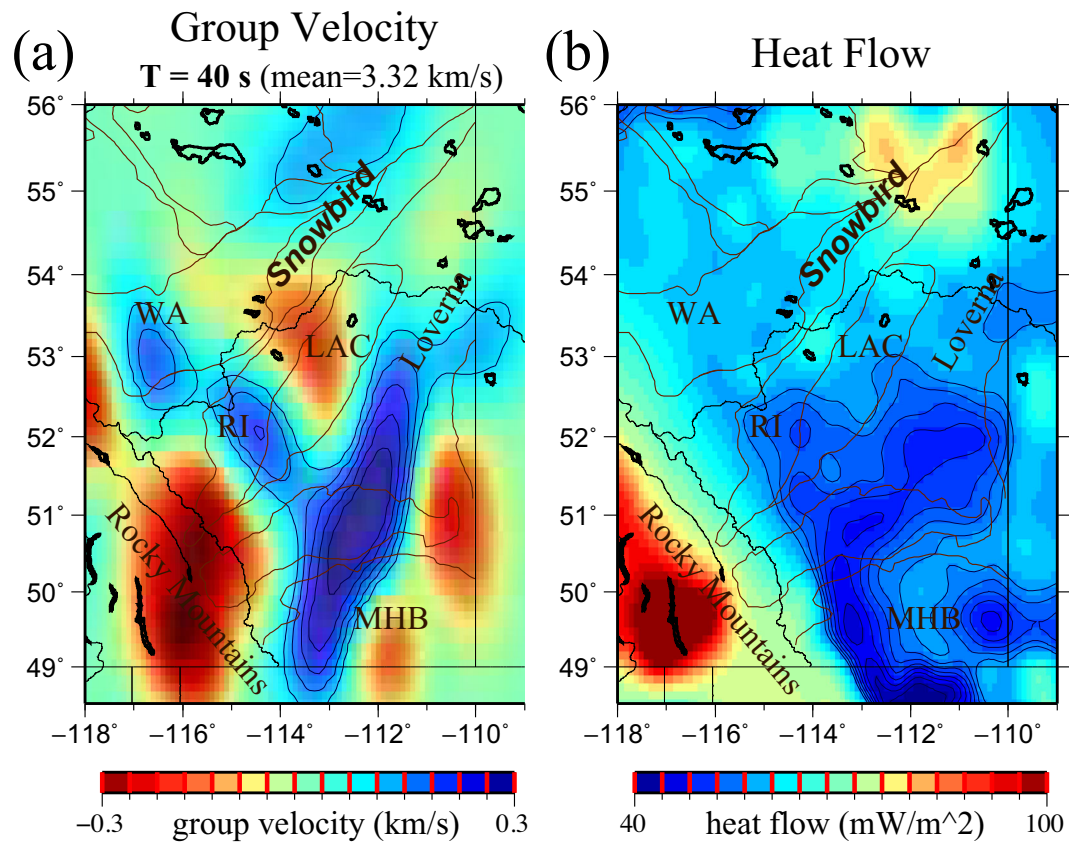


Figure 14. A comparison between regional heat flow (Blackwell & Richards 2004) and the group velocity map from the centre period of 40 s. A major Y-shaped high velocity structure approximately overlaps with zones of reduced heat flow. The acronym ‘LAC’ corresponds to the Lacombe domain. The remaining symbols are defined in Fig. 1.

A potential support for the presence of a large-scale seismic anomaly is heat flow data (Fig. 14). Based largely on borehole and breakout measurements, Blackwell & Richards (2004) published the heat flow map of the WCSB and was recently updated by Majorowicz *et al.* (2014). Only modest correlations are obtained with the inverted group velocity maps for period ranges of 6–23 s, but the absolute correlation coefficient between heat flow and velocities from the longest period exceeds 0.6. The shapes and orientations of major heat flow anomalies beneath southern Alberta Basin (low) and Rocky Mountains (high) are in excellent agreement with those of the group velocities. It has long been suggested that heat flow from Archean cratons is lower than that from younger Precambrian and Phanerozoic terrains (Ballard *et al.* 1987) on the global scale (Morgan 1985; Blackwell & Steele 1992; Holbrook *et al.* 1992; Christensen & Mooney 1995). According to these earlier studies, localized minima often coincide with Archean cratons and heat flow values increase by 20–25 per cent on average (Lenardic 1997; Rudnick *et al.* 1998; Rudnick & Gao 2003; Mareschal & Jaupart 2013) beneath Proterozoic domains. Similar trends are reported for a wide range of geological provinces and settings: for example, modest values of heat flow are detected from Archean crust in Baltic Shield (Mareschal & Jaupart 2013), South Africa (Ballard & Pollack 1986; Ballard *et al.* 1987; Rudnick *et al.* 1998; James & Fouch 2002), Australia (Neumann *et al.* 2000) and India (Gupta *et al.* 1993). Signatures from the Archean and younger domains in North America are more complex (Jaupart *et al.* 1998) where the measured heat flow from the Proterozoic Trans-Hudson Orogen is comparable to, or lower than, those bearing Archean signatures in eastern Canada (Rolandone *et al.* 2002; Perry *et al.*

2006). An unbiased assessment of regional surface heat flow in relation to crustal age remains a work-in-progress in Southwest WCSB. Further constraints on heat production (Ballard *et al.* 1987; Christensen & Mooney 1995; Rudnick *et al.* 1998; Perry *et al.* 2006)—a potentially correlated parameter as heat flow (Ballard *et al.* 1987; Rudnick *et al.* 1998; Perry *et al.* 2006), as well as the thermal state and root depth of the lithosphere (Lenardic 1997; Perry *et al.* 2006) would be needed. Nevertheless, the concordant low heat flow zone and high lower-crustal shear velocities in southern Alberta, which sharply contrasts with low mid-crustal velocities beneath the Cordillera (see Fig. 12; Kao *et al.* 2013), could be evidence for the existence of a relic Archean lower crustal/shallow mantle structure with modest heat production.

Combining all key observations from the lower crust, for example, high velocities beneath the Wabamun domain and Hearne province as well as intermittent low velocities along the Snowbird TZ, a strong argument could be made for a largely intact lower crust beneath Southwest WCSB from the Proterozoic eon. This finding is a major contrast to those from the upper crust where low velocity zones dominate the residual signatures, if any, from the presumed tectonic domains. The implication is that the proposed dual subduction during the Palaeoproterozoic era (see Fig. 1) has a major impact on the present-day upper crustal structure, but the boundary zones and major Archean/Proterozoic microplates are reasonably well preserved in the lower crust in Southwest WCSB.

The validation of potential connections between the Hearne province and the Medicine Hat Block would require a higher imaging resolution than that achievable by this study south of the US-Canada Border. For instance, based on the earlier SAREX

experiment, western Medicine Hat Block poses the fastest relative P -wave traveltimes in the crust (Clowes *et al.* 2002). However, the above-average velocities beneath the Medicine Hat Block in this study are mainly concentrated near the centre of the southern Loverna block-Vulcan Structure-Medicine Hat Block junction. The limited thickness (~ 8 km) of the proposed HLCL by (Lemieux *et al.* 2000) may negatively impact the layer detectability due to strong depth averaging in surface waves. Still, the contrasting average lower crustal/upper mantle velocities between eastern (slow) and western central (fast) Medicine Hat Block (see Figs 7 and 12) require a satisfactory explanation. Barring significant tectonic reworking during the Phanerozoic era, such differences would favor the Medicine Hat Block as the amalgamation of an Archean western-central fragment, which is connected to the Hearne province, and a distinctively younger/slower eastern segment. In view of the nearby Eyehill High, the latter segment was likely formed in connection with the Trans-Hudson Orogen during the Proterozoic eon.

6 CONCLUSIONS

This study presents a new crustal shear velocity model of Southwest WSCB based on the cross-correlation of ambient seismic noise. The best-constrained part of the model is south of the Lesser Slave Lake where the following key observations and conclusions are attained:

(1) Below-average upper crustal velocities are identified beneath southern-central Alberta, which covers an area ranging from Proterozoic accreted terranes (southeastern Wabamun domain) to Archean microcontinents (e.g. the Loverna Block). There is no concrete evidence for the connection between domain boundaries and upper crustal shear velocities; compositional variations in connection with Proterozoic subduction are likely responsible.

(2) A pronounced high velocity zone is identified in southern Loverna Block as well as the Wabamun domain. The orientation and amplitude of this anomaly are evidence for the existence of intact cores of the Archean Hearne province, which potentially underwent a clockwise rotation. The correlation between heat flow data and shear velocity suggests a relatively relic lower crust from the Proterozoic eon. In addition, anomalously high lower-crustal velocities from the Loverna Block extend into the Medicine Hat Block, which suggest extensive communications between the latter domain and the Hearne province.

Overall, the results of ambient noise tomography reveal complex crustal structures and domains in Alberta. While the origins of many observed features remain largely speculative, the improved data coverage based on regional arrays since 2006 does, and will continue to, provide critical insights into the formation and evolution of western Laurentia.

ACKNOWLEDGEMENTS

We thank Ruijia Wang, Yunfeng Chen and Yuanyin Zhang for insightful scientific suggestions and extensive help in editing of this manuscript. We thank Larry Heaman and Tom Chacko for helpful consultations on the tectonic history of the WSCB. We also thank two anonymous reviewers for their suggestions and comments, as well as the Editorial office and the Associate Editor for their support and professional handling of this manuscript. The staff members at CNSN and IRIS have been greatly assisted our efforts in seismic data acquisition. Above all, we are grateful to the host families of CRANE seismic stations for their support of our field project. This study is funded by Helmholtz-Alberta Ini-

tiative and the Canadian Foundation for Innovations (CFI). Several figures used in this paper were made using Generic Mapping Tools (Wessel & Smith 1998; <http://gmt.soest.hawaii.edu>, last accessed May 2012).

REFERENCES

- Ammon, C.J., Randall, G.E. & Zandt, G., 2012. On the nonuniqueness of receiver function inversions, *J. geophys. Res.*, **95**, 15 303–15 318.
- Aspler, L.B., Chiarenzelli, J.R. & McNicoll, V.J., 2002. Paleoproterozoic basement-cover infolding and thick-skinned thrusting in hearne domain, nunavut, canada: Intracratonic response to trans-hudson orogen, *Precambrian Res.*, **116**, 331–354.
- Aster, R.C., Borchers, B. & Thurber, C.H., 2013. *Parameter Estimation and Inverse Problems*, Academic Press, 376 pp.
- Aulbach, S., Griffin, W., O'Reilly, S. & McCandless, T.E., 2004. Genesis and evolution of the lithospheric mantle beneath the buffalo head Terrane, Alberta (Canada), *Lithos*, **77**, 413–451.
- Ballard, S. & Pollack, H.N., 1986. Diversion of heat by Archean cratons: a model for southern Africa, *Earth planet. Sci. Lett.*, **85**, 253–264.
- Ballard, S., Pollack, H.N. & Skinner, N.J., 1987. Terrestrial heat flow in Botswana and Namibia, *J. geophys. Res.*, **92**, 6291–6300.
- Banas, A., Stachel, T., Muehlenbachs, K. & McCandless, T.E., 2007. Diamonds from the Buffalo Head Hills, Alberta: formation in a non-conventional setting, *Lithos*, **93**, 199–213.
- Barton, P., 1986. The relationship between seismic velocity and density in the continental crust—a useful constraint?, *Geophys. J. Int.*, **87**, 195–208.
- Beaumont, C., Fullsack, P. & Hamilton, J., 1994. Styles of crustal deformation in compressional orogens caused by subduction of the underlying lithosphere, *Tectonophysics*, **232**, 119–132.
- Bensen, G., Ritzwoller, M. & Shapiro, N., 2008. Broadband ambient noise surface wave tomography across the United States, *J. geophys. Res.*, **113**, doi:10.1029/2007JB005248.
- Berman, R., Davis, W. & Pehrsson, S., 2007. Collisional snowbird tectonic zone resurrected: growth of Laurentia during the 1.9 Ga accretionary phase of the Hudsonian orogeny, *Geology*, **35**, 911–914.
- Berman, R.G. & Bostock, H.H., 1997. Metamorphism in the northern Tahsison magmatic zone, northwest Territoriesx, *Ganadian Mineralogis*, **35**, 1069–1091.
- Bickford, M., Collerson, K. & Lewry, J., 1994. Crustal history of the Rae and Hearne provinces, Southwestern Canadian shield, Saskatchewan: constraints from geochronologic and isotopic data, *Precambrian Res.*, **68**, 1–21.
- Blackwell, D. & Richards, M., 2004. Geothermal map of North America, *Am. Assoc. Petro. Geol.* (AAPG), 1 sheet, scale 1:6 500 000.
- Blackwell, D.D. & Steele, J.L., eds, 1992. DNAG geothermal map of North America, 1:5,000,000, 4 sheets, *Geol. Soc. Amer.*, Boulder, Co.
- Boerner, D., Kurtz, R., Craven, J., Rondenay, S. & Qian, W., 1995. Buried proterozoic foredeep under the western Canada sedimentary basin?, *Geology*, **23**, 297–300.
- Boerner, D., Craven, J., Kurtz, R., Ross, G. & Jones, F., 1998. The great falls tectonic zone: suture or intracontinental shear zone?, *Can. J. Earth Sci.*, **35**, 175–183.
- Boerner, D., Kurtz, R., Craven, J., Ross, G., Jones, F. & Davis, W., 1999. Electrical conductivity in the Precambrian lithosphere of western Canada, *Science*, **283**, 668–670.
- Boerner, D., Kurtz, R., Craven, J., Ross, G. & Jones, F., 2000. A synthesis of electromagnetic studies in the lithoprobe alberta basement transect: constraints on paleoproterozoic indentation tectonics, *Can. J. Earth Sci.*, **37**, 1509–1534.
- Bouzidi, Y., Schmitt, D.R., Burwash, R.A. & Kanasewich, E.R., 2002. Depth migration of deep seismic reflection profiles: crustal thickness variations in Alberta, *Can. J. Earth Sci.*, **39**, 331–350.
- Brocher, T.M., 2005. Empirical relations between elastic wavespeeds and density in the Earth's crust, *Bull. seism. Soc. Am.*, **95**, 2081–2092.
- Brzak, K., Gu, Y.J., Okeler, A., Steckler, M. & Lerner-Lam, A., 2009. Migration imaging and forward modeling of microseismic noise

- sources near southern Italy, *Geochem. Geophys. Geosyst.*, **10**, Q01012, doi:10.1029/2008GC002234.
- Burwash, R. & Culbert, R., 1976. Multivariate geochemical and mineral patterns in the Precambrian basement of western Canada, *Can. J. Earth Sci.*, **13**, 1–18.
- Burwash, R. & Krupička, J., 1969. Cratonic reactivation in the Precambrian basement of western Canada. I. Deformation and chemistry, *Can. J. Earth Sci.*, **6**, 1381–1396.
- Burwash, R. & Krupička, J., 1970. Cratonic reactivation in the Precambrian basement of western Canada. Part II. Metasomatism and isostasy, *Can. J. Earth Sci.*, **7**, 1275–1294.
- Burwash, R.A., Krupička, J. & Wijbrans, J.R., 2000. Metamorphic evolution of the Precambrian basement of Alberta, *Canadian Mineralogist*, **38**, 423–434.
- Canil, D., Schulze, D., Hall, D., Hearn, B. Jr. & Milliken, S., 2003. Lithospheric roots beneath western Laurentia: the geochemical signal in mantle garnets, *Can. J. Earth Sci.*, **40**, 1027–1051.
- Cassidy, J.F., 1995. A comparison of the receiver structure beneath stations of the Canadian National Seismograph Network, *Can. J. Earth Sci.*, **32**, 938–951.
- Chen, Y., Gu, Y.J., Dokht, R.H. & Sacchi, M., 2015. Crustal imprints of Precambrian orogenesis in western Laurentia, *J. geophys. Res.*, in press.
- Christensen, N.I. & Mooney, W.D., 1995. Seismic velocity structure and composition of the continental crust: a global view, *J. geophys. Res.*, **100**, 9761–9788.
- Clowes, R.M., Burianyk, M.J., Gorman, A.R. & Kanasewich, E.R., 2002. Crustal velocity structure from Sarex, the southern Alberta refraction experiment, *Can. J. Earth Sci.*, **39**, 351–373.
- Cook, F., Türkoglu, E., Unsworth, M. & Pana, D., 2009. Deep electrical structure of northern Alberta (Canada): Implications for diamond exploration, *Can. J. Earth Sci.*, **46**, 139–154.
- Courtier, A.M., Gaherty, J.B., Revenaugh, J., Bostock, M.G. & Garnero, E.J., 2010. Seismic anisotropy associated with continental lithosphere accretion beneath the canoe array, Northwestern Canada, *Geology*, **38**, 887–890.
- Cristiano, L., Petrosino, S., Saccorotti, G., Ohrnberger, M. & Scarpa, R., 2010. Shear-wave velocity structure at Mt. Etna from inversions of Rayleigh-wave dispersion patterns ($2 \text{ s} < T < 20 \text{ s}$), *Ann. Geophys.*, **52**(2), doi:10.4401/ag-4574.
- Crocker, C., Collerson, K., Lewry, J. & Bickford, M., 1993. Sm-Nd, U-Pb, and Rb-Sr geochronology and lithostructural relationships in the southwestern Rae province: constraints on crustal assembly in the western Canadian shield, *Precambrian Res.*, **61**, 27–50.
- Dalton, C.A., Gaherty, J.B. & Courtier, A.M., 2011. Crustal vs structure in northwestern Canada: imaging the cordillera-craton transition with ambient noise tomography, *J. geophys. Res.*, **116**, doi:10.1029/2011JB008499.
- De, S.K., Chacko, T., Creaser, R.A. & Muehlenbachs, K., 2000. Geochemical and Nd-Pb-O isotope systematics of granites from the Talson magmatic zone, Alberta: implications for early Proterozoic tectonics in western Laurentia, *Precambrian Res.*, **102**, 221–249.
- Dziewonski, A.M. & Anderson, D., 1981. Preliminary reference Earth model, *Phys. Earth. planet. Inter.*, **25**, 297–356.
- Dziewonski, A.M. & Hales, A.L., 1972. Numerical analysis of dispersed seismic waves, *Methods Comput. Phys.*, **11**, 39–85.
- Dziewonski, A.M., Bloch, S. & Landisman, M., 1969. Surface wave ray tracing azimuthal anisotropy: a generalized spherical harmonic approach technique for the analysis of dispersed seismic waves, *Bull. seism. Soc. Am.*, **59**, 427–444.
- Eaton, D.W. & Cassidy, J.F., 1996. A relic Proterozoic subduction zone in western Canada: new evidence from seismic reflection and receiver function data, *Geophys. Res. Lett.*, **23**, 3791–3794.
- Eaton, D.W., Ross, G.M. & Clowes, R.M., 1999. Seismic-reflection and potential-field studies of the Vulcan structure, western Canada: a Paleo-proterozoic Pyrenees, *J. geophys. Res.*, **104**, 23 255–23 269.
- Eaton, D.W., Ross, G.M. & Hope, J., 1999. The rise and fall of a cratonic arch: a regional seismic perspective on the Peace River arch, Alberta, *Bull. Can. Petrol. Geol.*, **47**, 346–361.
- Eaton, D.W., Ross, G.M., Cook, F.A. & VanderVelden, A., 2000. Seismic imaging of the upper mantle beneath the Rocky Mountain foreland, southwestern Alberta, *Can. J. Earth Sci.*, **37**, 1493–1507.
- Edwards, D.J. & Brown, R.J., 1999. Understanding the influence of Precambrian crystalline basement on upper Devonian carbonates in central Alberta from a geophysical perspective, *Bull. Can. Petrol. Geol.*, **47**, 412–438.
- Feng, M., Assumpcao, M. & Van der Lee, S., 2004. Group-velocity tomography and lithospheric S-velocity structure of the South American continent, *Phys. Earth planet. Inter.*, **147**, 315–331.
- Flowers, R., Bowring, S. & Williams, M., 2006. Timescales and significance of high-pressure, high-temperature metamorphism and mafic dike Anatexis, snowbird tectonic zone, Canada, *Contrib. Mineral. Petrol.*, **151**, 558–581.
- French, S., Fischer, K., Syracuse, E. & Wysession, M., 2009. Crustal structure beneath the Florida-to-Edmonton broadband seismometer array, *Geophys. Res. Lett.*, **36**, L08309, doi:10.1029/2008GL036331.
- Frost, C. & Burwash, R., 1986. Nd evidence for extensive Archean basement in the Western Churchill Province, Canada, *Can. J. Earth Sci.*, **23**, 1433–1437.
- Gorman, A.R. et al., 2002. Deep probe: imaging the roots of western North America, *Can. J. Earth Sci.*, **39**, 375–398.
- Gu, Y.J. & Shen, L., 2012. Microseismic noise from large ice-covered lakes, *Bull. seism. Soc. Am.*, **102**, 1155–1166.
- Gu, Y.J., Dublankov, C., Lerner-Lam, A., Brzak, K. & Steckler, M., 2007. Probing the sources of ambient seismic noise beneath Southern Italy, *Geophys. Res. Lett.*, **34**, L22315, doi:10.1029/2003GL031967.
- Gu, Y.J., Okeler, A., Shen, L. & Contenti, S., 2011. The Canadian Rockies and Alberta network (Crane): new constraints on the Rockies and western Canada sedimentary basin, *Seism. Res. Lett.*, **82**, 575–588.
- Gubbins, D., 2004. *Time Series Analysis and Inverse Theory for Geophysicists*, Cambridge Univ. Press, 255 pp.
- Gupta, M., Sundar, A., Sharma, S. & Singh, S., 1993. Heat flow in the Bastar Craton, central Indian shield: implications for thermal characteristics of proterozoic cratons, *Phys. Earth planet. Inter.*, **78**, 23–31.
- Gutenberg, G., 1951. Observation and theory of microseisms, in *Compendium of Meteorology*, pp. 1303–1311, ed. Malone, T.F., Am. Meteorol. Soc.
- Hanmer, S., Williams, M. & Kopf, C., 1995a. Striding-Athabasca Mylonite zone: implications for the Archean and early proterozoic tectonics of the western Canadian shield, *Can. J. Earth Sci.*, **32**, 178–196.
- Henstock, T.J. et al., 1998. Probing the Archean and proterozoic lithosphere of western North America, *GSA Today*, **8**, 1–5.
- Herrmann, R.B., 1987. Broadband Lg magnitude, *Seism. Res. Lett.*, **58**, 125–133.
- Herrmann, R.B., 2013. Computer programs in seismology: an evolving tool for instruction and research, *Seism. Res. Lett.*, **84**, 1081–1088.
- Hoffman, P.F., 1988. United plates of America, the birth of a Craton-early Proterozoic assembly and growth of Laurentia, *Ann. Rev. Earth planet. Sci.*, **16**, 543–603.
- Hoffman, P.F., 1990. Subdivision of the Churchill Province and extent of the trans-Hudson Orogen, in *The Early Proterozoic Trans-Hudson Orogen of North America*, Vol. 37, pp. 15–39, eds Lewry, J.F. & Stauffer, M.R., Geological Association of Canada, Special Paper.
- Holbrook, W.S., Mooney, W.D. & Christensen, N.I., 1992. The seismic velocity structure of the deep continental crust, *Continental Lower Crust*, **23**, 1–43.
- Hope, J. & Eaton, D., 2002. Crustal structure beneath the western Canada sedimentary basin: constraints from gravity and magnetic modelling, *Can. J. Earth Sci.*, **39**, 291–312.
- James, D. & Fouch, M., 2002. Formation and evolution of Archean Cratons: insights from southern Africa, *Special Publication-Geological Society of London*, **199**, 1–26.
- Jaupart, C., Mareschal, J.-C., Guillou-Frottier, L. & Davaille, A., 1998. Heat flow and thickness of the lithosphere in the Canadian shield, *J. geophys. Res.*, **103**, 15 269–15 286.

- Jones, A.G., Snyder, D., Hanmer, S., Asudeh, I., White, D., Eaton, D. & Clarke, G., 2002. Magnetotelluric and teleseismic study across the snowbird tectonic zone, Canadian shield: a Neoarchean mantle suture?, *Geophys. Res. Lett.*, **29**, 1011–1014.
- Jones, A.G. *et al.*, 2005. The electrical resistivity structure of Archean to tertiary lithosphere along 3200 km of Snorcle profiles, Northwestern Canada, *Can. J. Earth Sci.*, **42**, 1257–1275.
- Kanasewich, E., Clowes, R. & McCloughan, C., 1969. A buried Precambrian rift in western Canada, *Tectonophysics*, **8**, 513–527.
- Kanasewich, E., Burianyk, M., Dubuc, G., Lemieux, J. & Kalantzis, F., 1995. Three-dimensional seismic reflection studies of the Alberta basement, *Can. J. Explor. Geophys.*, **31**, 1–10.
- Kao, H. *et al.*, 2013. Ambient seismic noise tomography of Canada and adjacent regions: part I. Crustal structures, *J. geophys. Res.*, **118**, 5865–5887.
- Kim, S., Nyblade, A.A., Rhie, J., Baag, C.-E. & Kang, T.-S., 2012. Crustal S-wave velocity structure of the main Ethiopian rift from ambient noise tomography, *Geophys. J. Int.*, **191**, 865–878.
- Knopoff, L. & Schwab, F.A., 1968. Apparent initial phase of a source of Rayleigh waves, *J. geophys. Res.*, **73**, 755–760.
- Larson, E.W.F. & Ekström, G., 2001. Global models of surface wave group velocity, *Pure appl. Geophys.*, **158**, 1377–1399.
- Lemieux, S., Ross, G.M. & Cook, F.A., 2000. Crustal geometry and tectonic evolution of the Archean crystalline basement beneath the southern Alberta plains, from new seismic reflection and potential-field studies, *Can. J. Earth Sci.*, **37**, 1473–1491.
- Lenardic, A., 1997. On the heat flow variation from Archean cratons to proterozoic mobile belts, *J. geophys. Res.*, **102**, 709–721.
- Levshin, A.L., Pisarenko, V.F. & Pogrebinsky, G.A., 1972. On a frequency-time analysis of oscillations, *Ann. Geophys.*, **128**, 211–218.
- Levshin, A.L., Yanovskaya, T.B., Lander, A.V., Bukchin, B.G., Barmin, M.P., Ratnikova, L.I. & Its, E.N., 1989. Surface waves in vertically inhomogeneous media, in *Seismic Surface Waves in a Laterally Inhomogeneous Earth*, pp. 131–182, ed. Keilis-Borok, V.I., Kluwer.
- Lewry, J.F. & Sibbald, T.I., 1980. Thermotectonic evolution of the Churchill Province in northern Saskatchewan, *Tectonophysics*, **68**, 45–82.
- Lin, F.-C., Moschetti, M.P. & Ritzwoller, M.H., 2008. Surface wave tomography of the western United States from ambient seismic noise: Rayleigh and love wave phase velocity maps, *Geophys. J. Int.*, **173**, 281–298.
- Longuet-Higgins, M.S., 1950. A theory on the origin of microseisms, *Phil. Trans. R. Soc. Lond.*, **243**, 1–35.
- Ludwig, W.J., Nafe, J.E. & Drake, C.L., 1970. Seismic refraction, in *The Sea*, Vol. 4, pp. 53–84, ed. Maxwell, A.E., Wiley-Interscience.
- Mahan, K. & Williams, M., 2005. Reconstruction of a large deep-crustal terrane: implications for the snowbird tectonic zone and early growth of Laurentia, *Geology*, **33**, 385–388.
- Majorowicz, J. *et al.*, 2014. The first deep heat flow determination in crystalline basement rocks beneath the Western Canadian Sedimentary Basin, *Geophys. J. Int.*, **197**, 731–747.
- Mareschal, J.-C. & Jaupart, C., 2013. Radiogenic heat production, thermal regime and evolution of continental crust, *Tectonophysics*, **609**, 524–534.
- McDonough, M.R., McNicoll, V.J., Schetselaar, E.M. & Grover, T.W., 2000. Geochronological and kinematic constraints on crustal shortening and escape in a two-sided oblique-slip collisional and magmatic Orogen, paleoproterozoic Talton magmatic zone, northeastern Alberta, *Can. J. Earth Sci.*, **37**, 1549–1573.
- McNicoll, V.J., Theriault, J. & McDonough, M.R., 2000. Talton basement gneissic rocks: U-Pb and Nd isotopic constraints on the basement to the Paleoproterozoic Talton magmatic zone, northeastern Alberta, *Can. J. Earth Sci.*, **37**, 1575–1596.
- Mercier, J.P., Bostock, M., Audet, P., Gaherty, J., Garnero, E. & Revenaugh, J., 2008. The teleseismic signature of fossil subduction: northwestern Canada, *J. geophys. Res.*, **113**, doi:10.1029/2007JB005127.
- Mercier, J.-P., Bostock, M., Cassidy, J., Dueker, K., Gaherty, J., Garnero, E., Revenaugh, J. & Zandt, G., 2009. Body-wave tomography of western Canada, *Tectonophysics*, **475**, 480–492.
- Morgan, P., 1985. Crustal radiogenic heat production and the selective survival of ancient continental crust, *J. geophys. Res.*, **90**, C561–C570.
- Mueller, P.A., Heatherington, A.L., Kelly, D.M., Wooden, J.L. & Mogk, D.W., 2002. Paleoproterozoic crust within the great falls tectonic zone: implications for the assembly of southern Laurentia, *Geology*, **30**, 127–130.
- Neumann, N., Sandiford, M. & Foden, J., 2000. Regional geochemistry and continental heat flow: implications for the origin of the South Australian heat flow anomaly, *Earth planet. Sci. Lett.*, **183**, 107–120.
- Perry, H., Jaupart, C., Mareschal, J.C. & Bienfait, G., 2006. Crustal heat production in the Superior province, Canadian shield, and in North America inferred from heat flow data, *J. geophys. Res.*, **111**, doi:10.1029/2005JB003893.
- Rawlinson, N. & Cambridge, M., 2005. The fast marching method: an effective tool for tomographic imaging and tracking multiple phases in complex layered media, *Explor. Geophys.*, **36**, 341–350.
- Ritzwoller, M.H., Lin, F.-C. & Shen, W., 2011. Ambient noise tomography with a large seismic array, *Comptes Rendus Geosci.*, **343**, 558–570.
- Rolandone, F., Jaupart, C., Mareschal, J., Gariépy, C., Bienfait, G., Carbone, C. & Lapointe, R., 2002. Surface heat flow, crustal temperatures and mantle heat flow in the Proterozoic trans-Hudson Orogen, Canadian shield, *J. geophys. Res.*, **107**, 7–19.
- Ross, G., Parrish, R., Villeneuve, M. & Bowring, S., 1991. Geophysics and geochronology of the crystalline basement of the Alberta basin, western Canada, *Can. J. Earth Sci.*, **28**, 512–522.
- Ross, G.M., 2000. Introduction to special issue of Canadian journal of Earth sciences: the Alberta basement transect of Lithoprobe, *Can. J. Earth Sci.*, **37**, 1447–1452.
- Ross, G.M. & Eaton, D.W., 1997. Winagami reflection sequence: seismic evidence for postcollisional magmatism in the proterozoic of western Canada, *Geology*, **25**, 199–202.
- Ross, G.M. & Eaton, D.W., 1999. Basement reactivation in the Alberta basin: observational constraints and mechanical rationale, *Bull. Can. Petrol. Geol.*, **47**, 391–411.
- Ross, G.M. & Eaton, D.W., 2002. Proterozoic tectonic accretion and growth of western Laurentia: results from lithoprobe studies in northern Alberta, *Can. J. Earth Sci.*, **39**, 313–329.
- Ross, G.M., Milkereit, B., Eaton, D., White, D., Kanasewich, E.R. & Burianyk, M.J., 1995. Paleoproterozoic collisional Orogen beneath the western Canada sedimentary basin imaged by lithoprobe crustal seismic-reflection data, *Geology*, **23**, 195–199.
- Ross, G.M., Eaton, D.W., Boerner, D.E. & Miles, W., 2000. Tectonic entrapment and its role in the evolution of continental lithosphere: an example from the Precambrian of western Canada, *Tectonics*, **19**, 116–134.
- Rudnick, R. & Gao, S., 2003. Composition of the continental crust, *Treatise Geochem.*, **3**, 1–64.
- Rudnick, R.L., McDonough, W.F. & O'Connell, R.J., 1998. Thermal structure, thickness and composition of continental lithosphere, *Chem. Geol.*, **145**, 395–411.
- Sabra, K.G., Gerstoft, P., Roux, P., Kuperman, W. & Fehler, M.C., 2005. Surface wave tomography from microseisms in southern California, *Geophys. Res. Lett.*, **32**, doi:10.1029/2005GL023155.
- Saygin, E. & Kennett, B.L., 2010. Ambient seismic noise tomography of Australian continent, *Tectonophysics*, **481**, 116–125.
- Saygin, E. & Kennett, B., 2012. Crustal structure of Australia from ambient seismic noise tomography, *J. geophys. Res.*, **117**, doi:10.1029/2011JB008403.
- Schivardi, R. & Morelli, A., 2009. Surface wave tomography in the European and Mediterranean region, *Geophys. J. Int.*, **177**, 1050–1066.
- Schultz, R., Stern, V. & Gu, Y.J., 2014. An investigation of seismicity clustered near the Cordel Field, west central Alberta, and its relation to a nearby disposal well, *J. geophys. Res.: Solid Earth*, **119**, doi:10.1002/2013JB010836.
- Shapiro, N.M., Campillo, M., Stehly, L. & Ritzwoller, M.H., 2005. High-resolution surface-wave tomography from ambient seismic noise, *Science*, **307**, 1615–1618.
- Shragge, J., Bostock, M., Bank, C. & Ellis, R., 2002. Integrated teleseismic studies of the southern Alberta upper mantle, *Can. J. Earth Sci.*, **39**, 399–411.

- Thériault, R. & Ross, G., 1991. Nd isotopic evidence for crustal recycling in the ca. 2.0 Ga subsurface of western Canada, *Can. J. Earth Sci.*, **28**, 1140–1147.
- Thomas, M., Sharpton, V. & Grieve, R., 1987. Gravity patterns and Precambrian structure in the North American central plains, *Geology*, **15**, 489–492.
- Villeneuve, M., Ross, G., Parrish, R., Theriault, R., Miles, W. & Broome, J., 1993. Geophysical subdivision, U–Pb geochronology and Sm–Nd isotope geochemistry of the crystalline basement of the western Canada sedimentary basin, Alberta and Northeastern British Columbia, *Geol. Surv. Canada Bull.*, **447**, 1–86.
- Ward, K.M., Porter, R.C., Zandt, G., Beck, S.L., Wagner, L.S., Minaya, E. & Tavera, H., 2013. Ambient noise tomography across the Central Andes, *Geophys. J. Int.*, **194**, 1559–1573.
- Wessel, P. & Smith, W.H.F., 1998. New, improved version of the Generic Mapping Tools released, *EOS Trans., AGU*, **79**, 579, doi:10.1029/98EO00426.
- Yang, Y., Ritzwoller, M.H., Zheng, Y., Levshin, A.L. & Xie, Z., 2012. A synoptic view of the distribution and connectivity of mid-crustal low velocity zone beneath Tibet, *J. geophys. Res.*, **117**, B04303, doi:10.1029/2011JB008810.
- Yao, H., van Der Hilst, R.D. & Maarten, V., 2006. Surface-wave array tomography in SE Tibet from ambient seismic noise and two-station analysis—1. Phase velocity maps, *Geophys. J. Int.*, **166**, 732–744.
- Zelt, C. & White, D., 1995. Crustal structure and tectonics of the Southeastern Canadian cordillera, *J. geophys. Res.*, **100**, 24 255–24 273.
- Zelt, C.A. & Ellis, R., 1989. Seismic structure of the crust and upper mantle in the Peace River Arch region, Canada, *J. geophys. Res.*, **94**, 5729–5744.

SUPPORTING INFORMATION

Additional Supporting Information may be found in the online version of this article:

Figure S1. Distributions of travel time residuals from the SCCFs relative to the best-fitting regional average (see Fig. 4) for each period range. The majority of the residuals are Gaussian distributed with a standard deviation of ~ 3 s. Assuming an average interstation distance of 210 km and an average group velocity of 3 km s^{-1} (see Fig. 4), this translates to a 3–4 per cent error in group velocity measurements.

Figure S2. Normalized rms of noise. Two approaches are used in this estimation. In the first case, which is referred to as ‘noise variance’, each SCCF is first normalized to its maximum amplitude and the variance is computed using the normalized amplitudes in the lag time window of 400–500 s (which is outside of the expected Rayleigh wave window in view of the source–receiver distances used in this study). The resulting variances from all available station pairs are then averaged to produce a single value within given narrow (0.02-Hz wide) passband. This procedure produces 20 variance values for the entire period range from 0 to 70 s (see Fig. S2). The ‘data variance’ is computed using the same algorithm, with the exception that the variance value is computed based on the entire SCCF (with lag time window of 0–500 s). The mean values of the normalized rms across all period ranges and the five centre periods from this study are indicated on the plots.

Figure S3. Results of an iterative inversion for the 1-D shear velocity structure beneath sample point P4 (see Fig. 10a). The starting and inverted models are denoted by saturated blue and red colours, respectively. The limited range of variations in velocity is evidence for a stable inversion result.

Figure S4. (a)–(c) Shear velocities obtained using an initial model with a constant velocity of 3 km s^{-1} . The notations and selected depths are equivalent to those of Fig. 11. The large-scale velocities, particularly a low-velocity central Alberta and high-velocity Loverna Block–Vulcan Structure–Medicine Hat Block, are consistently resolved despite the substantial differences in the input models (see Fig. 11 for comparison). (d) Input (black) and regionally averaged inversion result (blue). The low velocity zone (see also Fig. 11d) is present below 15 km depth.

Figure S5. (a)–(c) Shear velocities obtained using variable initial 1-D models. (d) The base models (black) used to construct the initial 1-D structure. Also shown is the average 1-D structure from the output of the inversion (‘Out 2’, red) and that from a uniform starting model (‘Out 1’, blue). The initial model at each node is computed based on the weighted averages of 1-D models from nearby stations using receiver functions (Chen *et al.* 2015). Spherical B-splines with an averaging radius of 500 km are used as the weighting function. Hence, the initial model for each node is different, and should closely resemble the 1-D base structure under the nearest station. The resulting lateral velocity perturbations shown in panels (a) to (c)—the main targets of this study, are highly consistent with those from a uniform starting model (see Fig. 11d). Nonetheless, the average 1-D structure from variable initial models (‘Output 2’, same as ‘M2’ in Fig. 11d) is notably different from that of a uniform (‘Out 1’, same as ‘M1 Out’ in Fig. 11d) or a constant (same as ‘M0 Out’ in Fig. 11d, see also Fig. S4) initial model.

Figure S6. Shear velocities from a vertical resolution test and the cross-sections are the same as those shown in Figs 12 and 13. In this test, we compute the dispersion curve using a constant 1-D model of 3 km s^{-1} . Then Gaussian noise of 4 per cent ($\sim 0.12 \text{ km s}^{-1}$, see main text for reasoning) is added to each theoretical group velocity prior to the recovery test. The inversion utilizes the same inversion algorithm and regularization parameter as those deployed on the actual data. The output model shows considerable spatial variations, though the overall amplitude and pattern (or, the lack of thereof) are considerably different from those of a more realistic initial model (i.e. zonal). The largest perturbations shown in extreme dark and light colours do not coincide with our key observations of interests (e.g. fast velocities beneath the Loverna Block and low velocities under the Alberta basin) (<http://gji.oxfordjournals.org/lookup/suppl/doi:10.1093/gji/ggv100/-DC1>).

Please note: Oxford University Press is not responsible for the content or functionality of any supporting materials supplied by the authors. Any queries (other than missing material) should be directed to the corresponding author for the article.